

## Article

# Boron-Based Compounds for Solid-State Hydrogen Storage: A Review

Yernat Kozhakhmetov <sup>1</sup>, Sherzod Kurbanbekov <sup>2,\*</sup>, Nurya Mukhamedova <sup>3</sup> , Azamat Urkunbay <sup>1</sup>, Aibar Kizatov <sup>1</sup> ,  
Leila Bayatanova <sup>1</sup>, Raushan Nurdillayeva <sup>2</sup>  and Dilnoza Baltabayeva <sup>2</sup> 

<sup>1</sup> Center of Excellence “VERITAS”, NJSC «D. Serikbayev East Kazakhstan Technical University», Ust-Kamenogorsk 070004, Kazakhstan; ykozhakhmetov@edu.ektu.kz (Y.K.); urkunbay@gmail.com (A.U.); kizatov.aibar.sovetbekuly@gmail.com (A.K.); lbayatanova@edu.ektu.kz (L.B.)

<sup>2</sup> The Research Institute “Natural Sciences, Nanotechnology and New Materials”, Khoja Akhmet Yassawi International Kazakh-Turkish University, Turkestan 161200, Kazakhstan; raushan.nurdillayeva@ayu.edu.kz (R.N.); dilnoza.baltabayeva@ayu.edu.kz (D.B.)

<sup>3</sup> Institute of Atomic Energy Branch of the National Nuclear Center of the Republic of Kazakhstan, Kurchatov 071100, Kazakhstan; bakayeva@nnc.kz

\* Correspondence: sherzod.kurbanbekov@ayu.edu.kz

**Abstract:** Due to the depletion of hydrocarbon resources worldwide, intensive research is being conducted to identify alternative energy carriers. Hydrogen has emerged as a promising candidate due to its high energy density and environmentally friendly nature. However, large-scale implementation of hydrogen energy is hindered by the lack of safe, efficient, and cost-effective storage methods. Among the various materials studied for solid-state hydrogen storage, boron nitride (BN)-based compounds have attracted significant attention owing to their high thermal stability, tunable morphology, and potential for physisorption-based storage. This review focuses on recent advances in the synthesis, functionalization, and structural optimization of BN-based materials, including nanotubes, nanosheets, porous frameworks, and chemically modified BN. Although other boron-containing hydrides such as  $\text{LiBH}_4$ ,  $\text{Mg}(\text{BH}_4)_2$ , and closo-borates are briefly mentioned for comparison, the primary emphasis is placed on BN-related systems. This paper discusses various modification strategies aimed at enhancing hydrogen uptake and reversibility, offering insights into the future potential of BN-based materials in hydrogen storage technologies.

**Keywords:** hydrogen storage; boron-based compounds; boron nitride; h-BN



Academic Editor: Kaveh Edalati

Received: 15 April 2025

Revised: 26 May 2025

Accepted: 30 May 2025

Published: 3 June 2025

**Citation:** Kozhakhmetov, Y.; Kurbanbekov, S.; Mukhamedova, N.; Urkunbay, A.; Kizatov, A.; Bayatanova, L.; Nurdillayeva, R.; Baltabayeva, D. Boron-Based Compounds for Solid-State Hydrogen Storage: A Review. *Crystals* **2025**, *15*, 536. <https://doi.org/10.3390/cryst15060536>

**Copyright:** © 2025 by the authors. Licensee MDPI, Basel, Switzerland. This article is an open access article distributed under the terms and conditions of the Creative Commons Attribution (CC BY) license (<https://creativecommons.org/licenses/by/4.0/>).

## 1. Introduction

The world faces urgent problems related to preserving resources, producing energy efficiently, improving transportation, and ensuring long-term storage solutions. These challenges are exacerbated by environmental problems, particularly the increased release of carbon dioxide and other harmful gases, which are intensifying human impact on the climate [1,2].

As the world moves towards cleaner energy sources (decarbonization), scientific research is heavily focused on creating innovative, energy-efficient, and environmentally friendly technologies for the entire energy lifecycle, from production to consumption. Hydrogen is gaining significant attention as a potential energy carrier due to its high energy content, clean-burning properties, and diverse production methods [3].

Hydrogen, a pure and non-toxic element, can be produced from various sources like fossil fuels, biomass, and water, making it adaptable to different technologies. However,

challenges remain, especially in ensuring the reliability, efficiency, and safety of hydrogen storage and transportation. Therefore, considerable research is dedicated to developing new materials and designs that can effectively store hydrogen under realistic operating conditions [4].

Current hydrogen storage methods involve compressing it, liquefying it, or binding it to solid materials like carbon nanomaterials, boron and nitrogen compounds, metal–organic frameworks (MOFs), and covalent organic frameworks (COFs). Using these nanostructured materials, especially those enhanced with lithium, offers promising possibilities for developing compact, safe, and energy-efficient hydrogen storage systems [5–7].

In conclusion, hydrogen is a crucial element in the global shift towards sustainable energy. Continued research and development are essential to improve hydrogen storage technologies, transportation methods, and their integration into existing energy systems (Table 1) [7].

**Table 1.** Hydrogen storage methods [7].

	Storage Method	Advantages	Disadvantages
Physical methods	Compressed gaseous hydrogen (300 K, $\leq 200$ bar) stationary storage systems and underground repositories; glass microspheres and capillaries	Mature and accessible technology, relatively low cost	Low volumetric capacity ( $\sim 7.7$ kg/m <sup>3</sup> at 100 bar). High-pressure storage (up to 700 bar) remains underdeveloped.
	Liquid hydrogen (20.4 K)	High density (71 kg/m <sup>3</sup> )	High energy costs for liquefaction, hydrogen loss due to evaporation, need for superinsulation, high cost.
Storing hydrogen in its physical form, either as a liquefied gas at cryogenic temperatures or as a compressed gas under high pressure, allows for large volumes to be stored. However, this requires specialized equipment capable of withstanding extreme conditions, such as pressures of hundreds of megapascals and temperatures below the temperature of liquid nitrogen. Although technically feasible, these storage methods often prove to be disadvantageous in terms of cost, ease of use, and safety. Liquid hydrogen is stable only in a narrow temperature range between its boiling point (20 K) and freezing point (17 K). As the temperature rises above the boiling point, it rapidly evaporates and becomes a gas. Although the strength and material requirements for cryogenic liquid hydrogen tanks are less stringent than for pressure vessels used to store gaseous hydrogen, the gravimetric density of storage in liquid form is higher. However, the maximum bulk density is limited by the intrinsic density of liquid hydrogen, which is 70.8 kg/m <sup>3</sup> .			
Adsorption Methods	Cryoadsorption (activated carbon, 155 K)	Simple and well-developed technology	Low volumetric capacity (0.5–20 kg/m <sup>3</sup> ). Requires cooling and compression.
	Zeolites, MOFs	Low cost, scalable production, reusability, low losses (0.1%)	Low hydrogen capacity (Zeolites: $\sim 0.3$ wt.% at RT, 1.8 wt.% at 77 K; MOFs: 1 wt.% at RT, 4.5 wt.% at 70 K)
	Carbon nanostructures (nanotubes, fullerenes)	Technologies in the future can provide high Potential for high storage density (30–100 kg/m <sup>3</sup> )	Unreliable production methods, inconsistent hydrogen retention results.
Hydrogen storage systems that use physical sorption have high storage capacity for their size and weight at low pressures, are affordable, and are easy to build. Nonetheless, notable limitations exist, such as a low hydrogen capacity—spanning from 1 to 4.5 wt.%—and reduced sorption temperatures, which are generally at the temperature of liquid nitrogen. A common problem with how hydrogen is stored in various materials like metal–organic frameworks, zeolites, and carbon is that the energy holding hydrogen to the surface is not strong enough to allow for good storage at temperatures higher than that of liquid nitrogen.			

Table 1. Cont.

	Storage Method	Advantages	Disadvantages
Chemical Methods	Metal hydrides, intermetallics, composites	Safe solid-state storage, well-developed technologies	Limited capacity ( $\leq 1.5$ wt.%), heating required, degradation over time, high cost.
	Irreversible hydrides (AlH <sub>3</sub> , NH <sub>3</sub> , methanol) water-reactive (AlH <sub>3</sub> , Fe, Al, Si, water-regulating alloys based on aluminum and silicon, NH <sub>3</sub> , methanol, ethanol, etc.)	High volumetric density (~100 kg/m <sup>3</sup> )	Difficult to reuse storage media.

It is evident that the metal hydride method can successfully compete with conventional hydrogen storage methods in terms of compactness, but it is inferior to them in gravimetric performance. The hydrogen content by mass is significantly higher for high-temperature hydrides of light elements.

Each existing hydrogen storage method has specific advantages and limitations, which are influenced by both technical parameters (e.g., energy density, reversibility) and economic considerations in the target application. Among these, metal and complex hydrides stand out as promising candidates for hydrogen storage and transport due to their favorable safety profile, high volumetric density, and tunable thermodynamic properties [8].

Recent publications have extensively surveyed the field of hydrogen storage technologies, each emphasizing different materials or methodologies. For example, Usman and colleagues (2022) presented a comprehensive overview of hydrogen storage techniques, encompassing gaseous, liquid, and solid-state options. Their study underscores the fundamental difference between physical storage (compressed gas and cryogenic liquid) and material-dependent storage approaches like metal hydrides, physisorption materials, and chemical hydrogen carriers. The researchers highlighted that hydrogen can be stored through diverse physical and chemical processes, summarizing the pros and cons of each, especially regarding energy efficiency, safety considerations, and system complexity. However, their analysis omitted any discussion of boron nitride (BN) or hexagonal boron nitride (h-BN) materials [9].

Conversely, Scarpati et al. [10] specifically investigated metal hydrides for use in mobile systems, particularly fuel cell vehicles. Their review offers a thorough comparison of the most relevant metal hydrides, including their typical reversible hydrogen storage capacities (ranging from 1.3% to 1.85% by weight) and volumetric densities (approximately 90 g/L), along with reaction enthalpies spanning 25–35 kJ/mol H<sub>2</sub>. The authors emphasized the potential of metal hydrides for specialized transportation uses but acknowledged ongoing challenges related to weight, reaction kinetics, and stability over repeated cycles. Boron-containing or h-BN-based materials were not considered in this study.

Mahmoud et al. [11] analyzed porous carbon materials—such as graphene, activated carbons, and carbon nanotubes—for hydrogen storage based on physical adsorption principles. Their review examines how key material properties, including surface area, pore size distribution, and surface chemistry, influence hydrogen uptake under moderate pressure. The authors outlined several strategies, such as introducing heteroatoms and using nanostructuring, to improve both storage capacity and kinetics. Nevertheless, h-BN and other boron nitride-based systems were not included in their scope.

Similarly, Elyasi et al. [12] concentrated on nanoporous carbons derived from biomass for solid-state hydrogen storage. They highlighted the importance of pore structure and surface chemistry in optimizing hydrogen adsorption and desorption. Notably, the review mentions that incorporating heteroatoms—like boron, nitrogen, and sulfur—can enhance hydrogen interactions with carbon surfaces. While BN nanotubes are briefly mentioned

regarding enhanced binding energies, the main focus remains on carbonaceous materials and their modifications.

Soni et al. provided a critical assessment of carbon-based materials for hydrogen storage, covering activated carbon, carbon aerogels, graphene, graphite, fullerenes, carbon nanotubes, and MXenes. The review emphasizes recent engineering techniques aimed at increasing hydrogen uptake, such as tailoring pore size and functionalization. The authors underlined that, despite notable advancements, current carbon materials still do not meet practical requirements. BN or h-BN materials were not considered in their work [13].

Finally, Sutton et al. presented an in-depth analysis of metal–organic frameworks (MOFs) for hydrogen storage at or near room temperature. The review explores the limitations of typical MOF-H<sub>2</sub> interactions (heat of adsorption around 4–7 kJ/mol) and suggests methods to improve binding energy using open metal sites, alkali metal doping, and hydrogen spillover mechanisms. While the study offers detailed comparisons of MOF performance and modification strategies, it does not address boron-containing or BN-based materials [14].

This review focuses on the potential of boron-containing materials, especially nanostructured boron nitride, as effective media for hydrogen adsorption, storage, and release. We provide a systematic analysis of recent experimental and theoretical studies, highlight key morphological modifications (e.g., doping, functionalization, porosity), and compare the performance of h-BN with other emerging storage materials. To the best of our knowledge, no recent review has comprehensively addressed the integration of various h-BN morphologies for hydrogen storage. Therefore, this work aims to fill that gap and contribute to the growing body of knowledge on boron-based hydrogen storage systems.

## 2. Key Properties of BN-Based Materials for Hydrogen Storage

BN-based materials, especially in nanostructured form (nanotubes, nanosheets, porous frameworks), are promising candidates for hydrogen storage due to their high-temperature and chemical stability, low density, high specific surface area (up to 1500 m<sup>2</sup>/g), and the ability to control porosity and surface chemistry through doping and functionalization. These properties allow BN materials to efficiently adsorb hydrogen at cryogenic temperatures (up to 2.6 wt.% at 77 K and 1 bar), while providing safe operation due to a wide band gap (~5.5 eV) and electrical insulation. In contrast to metal hydrides, which require high temperatures and have low reversibility, and carbon materials with limited capacity, BN provides an optimal balance between stability, safety, and the potential for improved hydrogen storage efficiency.

In the early 21st century, boron nitride (BN) attracted much attention as a promising hydrogen storage material. This is due to its outstanding physicochemical properties, such as high thermal and chemical stability, low density, developed porosity, and unique electronic properties. In 2002, Wang et al. [15] synthesized nanostructured hexagonal BN (h-BN) by mechanochemical milling in a hydrogen atmosphere. The resulting material demonstrated hydrogen absorption at a level of 2.6 wt.%, which is approximately 35% higher than that of nanostructured graphite, which was previously considered a reference adsorbent. Hydrogen desorption was observed at about 570 K and nitrogen desorption at about 700 K. No signs of recrystallization of the material were found even when heated to 1173 K. The differences in the behavior of h-BN and graphite during dehydrogenation are likely due to local differences in the electronic structure near the lattice defects [16].

Despite the favorable properties, the development of BN-based systems in the field of hydrogen storage lags behind other materials such as MOFs and borane ammine (NH<sub>3</sub>BH<sub>3</sub>) [17–24]. However, the results of computer simulations [25] open up new possibilities for modifying BN to create next-generation hydrogen storage technologies. This

promising research direction is attracting increasing attention, and the present work aims to critically evaluate the hydrogen storage potential of modified BN structures, explore conceptual strategies, and identify key issues.

BN frameworks are composed of equimolar amounts of boron (B) and nitrogen (N) atoms, forming structures that are isoelectronic to carbon lattices and have similar morphology. Among the polymorphs of BN, hexagonal BN (h-BN) is the most stable under ambient conditions [25], while cubic BN (c-BN), an analogue of diamond, is known for its exceptional hardness [25], and wurtzite BN (w-BN) is an  $sp^3$ -hybridized tetrahedral structure with various configurations [25]. Structurally, h-BN consists of layers in which B and N atoms are strongly bonded by covalent bonds, and interlayer interactions are due to weak van der Waals forces (Figure 1). However, unlike graphite, h-BN has an AB-type stacking, where the B atoms in one layer are located directly above the N atoms in adjacent layers, reflecting the polarity of the B-N bonds. The electron density is shifted towards the more electronegative N atoms, with only partial delocalization of the nitrogen pz electrons into the boron pz orbital, as opposed to the complete delocalization characteristic of the C-C bonds in graphite [25].

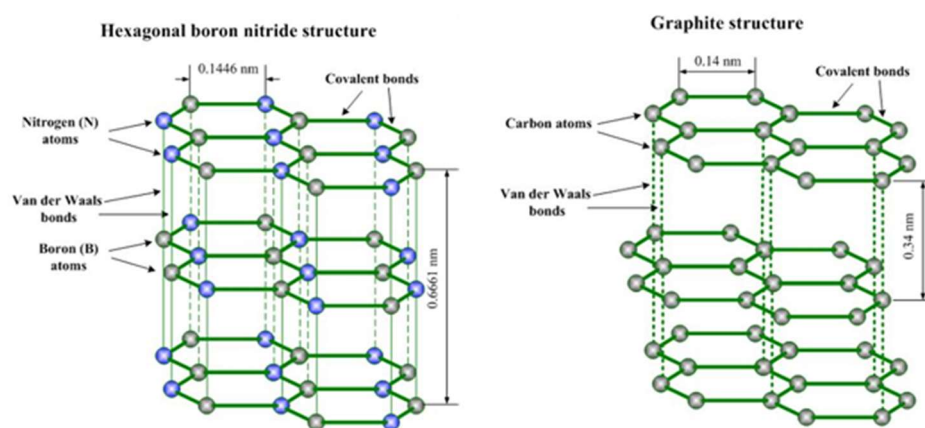


**Figure 1.** Structures of h-BN (left) and graphite (right). Reproduced from [www.substech.com](http://www.substech.com) [25].

Hexagonal boron nitride (h-BN) possesses remarkable physical and chemical properties due to its unique structure, including high thermal conductivity, mechanical strength, electrical insulation, and thermal/chemical stability. Its promising applications across diverse scientific and technological domains have made boron nitride-based materials a focus of current research. Boron nitride exists in various structural forms, including those analogous to carbon structures like diamond (c-BN), lonsdaleite (w-BN), and graphite (g-BN). Beyond these, BN can form nanosheets, nanotubes, and porous materials, thanks to the different bonding configurations ( $sp$ ,  $sp^2$ , and  $sp^3$  hybridization) of boron and nitrogen [26–28].

Like other cutting-edge substances, BN has been extensively examined in recent years concerning its nanostructured configurations and related characteristics. The progression of BN nanomaterials has mirrored that of their carbon equivalents, moving from zero-dimensional (0D) fullerenes and nanocages, and one-dimensional (1D) nanotubes in the 1990s, to two-dimensional (2D) graphene and nanosheets in the 2000s. This evolution also encompasses diverse forms like nanomeshes, nanospheres, nanowires, nanoribbons, and nanoporous BN [29].

The findings acquired by research teams exploring BN and carbon materials for hydrogen storage using density functional theory (DFT) calculations offer significant data for mathematical modeling of adsorption/desorption mechanisms. When evaluating the hydrogen storage capacity of solid-state substances, multiple parameters are considered,

including binding energy, adsorption energy, average adsorption energy, and desorption temperature. Based on computational modeling by scientists from Australia and the United States, boron nitrides are capable of storing between 6.5 and 8.65 weight percent of hydrogen. The simulations indicate that each gram of BN can reversibly adsorb and desorb up to 60 L of hydrogen.

Scientists have utilized diverse DFT-based computational software programs [30], including VASP, Quantumwise ATK, CASTEP, GAMESS, and Dmol3, to scrutinize hydrogen adsorption behaviors in BN and carbon nanostructures [31,32]. The following equation is used to calculate the adsorption energy [33,34]:

$$E_{ad} = E_{tot} \left( \frac{BN}{C} + H_2 \right) - E_{tot} \left( \frac{BN}{C} \right) - nE_{free}(H_2) \quad (1)$$

The average adsorption energy is calculated using the following relationship:

$$E_{ad} = \left\{ E_{tot} \left( \frac{BN}{C} + H_2 \right) - E_{tot} \left( \frac{BN}{C} \right) - nE_{free}(H_2) \right\} / n \quad (2)$$

where:

$\frac{BN}{C}$  denotes the base material of carbon and BN nanomaterials,  $E_{tot} \left( \frac{BN}{C} + H_2 \right)$ —is the total energy of hydrogen molecules adsorbed by the system,  $E_{free}(H_2)$ —is the total energy of a free  $H_2$  molecule.

$E_{tot} \left( \frac{BN}{C} \right)$ —the total energy of the base material (carbon and boron nitride nanostructures) is represented, with  $n$  indicating the quantity of adsorbed  $H_2$  molecules on the base materials.

The capacity of carbon and boron nitride nanomaterials to absorb hydrogen can be determined through the following equations [35–38]:

$$H_2(\text{wt}\%) = \frac{nM_{H_2}}{(nM_{H_2} + M_{Host})} \cdot 100 \quad (3)$$

where:

$M_{H_2}$ ,  $M_{Host}$  и  $n$ —and  $n$  are the masses of  $H_2$ , host material (boron nitride and carbon nanostructure), and the number of  $H_2$  molecules, respectively.

To quantitatively analyze the desorption process, the desorption temperature (TD(K)) is estimated using the Van't Hoff equation [39]:

$$T_D = \left( \frac{E_{ads}}{K_b} \right) \left( \frac{\Delta S}{R} - \ln P \right)^{-1} \quad (4)$$

where:

$K_b$ —Boltzmann constant ( $1.38 \times 10^{-23} \text{ J K}^{-1}$ );

$\Delta S = 130 \text{ J K}^{-1} \text{ Mol}^{-1}$ —change in entropy of  $H_2$  from gas to liquid phase at equilibrium pressure  $P = 1 \text{ atm}$ ;

$R(=8.31 \text{ J K}^{-1} \text{ Mol}^{-1})$ —gas constant.

Ball milling primarily results in a substantial enlargement of the specific surface area, the creation of refined microstructures with smaller grain dimensions, the generation of numerous imperfections (both on the surface and within the bulk material) and phase interfaces, the formation of porous surface textures offering abundant locations for hydrogen absorption/desorption, a near-consistent hydrogen storage capability compared to the original material, faster hydrogenation rates, and enhanced thermodynamic attributes.

These microstructural defects act as points where the hydride phase begins to form, and the expanded boundary area makes it easier for hydrogen to diffuse. These changes

lead to improved surface activation and hydrogenation speed, decreased activation energy requirements, lower temperatures for hydrogen release, and faster movement of hydrogen within the material.

Modern metal hydride-based hydrogen storage systems (HSSs) are generally classified into the following categories: Alloys based on rare earth metals (REMs), including mischmetal alloys (which are mixtures of rare earth elements produced during the creation of pure REM), typically containing 25–35% La, 40–50% Ce, 4–15% Nd, 1–7% Sm+Gd, and unavoidable impurities such as Fe, Si, Mg, and Al; they also include alloys based on titanium, zirconium, and magnesium [40–43].

BN nanomaterials, similar to their carbon counterparts, possess notable porosity and elevated surface area. These characteristics, coupled with remarkable thermodynamic stability and chemical inertness (h-BN remains stable in air up to 1273 K), the high specific surface area of nanoparticles, and polar covalent B-N bonds, make them promising for various applications, especially hydrogen storage [44]. While recent theoretical studies increasingly emphasize the potential of BN-based structures for achieving high physisorption capacities, traditionally, h-BN materials have been primarily considered effective for hydrogen storage through chemisorption processes [45]. Hexagonal boron nitride (h-BN) is a very stable hydrogen storage material, offering superior performance, excellent cyclability, and regeneration capabilities. However, a significant obstacle to the industrial application of h-BN is the absence of well-defined, cost-effective methods for large-scale production of nanostructured forms, as well as the creation of straightforward and effective modification techniques to enhance sorption performance. The exceptional qualities of this material and its hydrogen storage potential are extensively reviewed in [46–51]. For instance, BN nanotubes synthesized through the annealing of ball-milled boron-nickel catalyst in a nitrogen/hydrogen gas mixture at 1298 K exhibited hydrogen sorption capabilities at room temperature, with a predicted storage capacity reaching up to 2.2 wt.% at 6 MPa pressure [52]. The improved hydrogen storage capabilities of this material can be attributed to its nanoscale structure and the existence of heteropolar B-N bonds. The ionic B-N bond generates an extra dipole moment, which enhances hydrogen adsorption strength.

Nanostructured BN possesses unique physical and chemical properties compared to bulk and micro-sized materials. For instance, BN nanoparticles (BNNPs) can be synthesized through precursor vapor-phase pyrolysis, then adapted into nanostructures by high-temperature annealing (2273 K). Subsequent ball milling of these nanostructures can further improve the specific surface area. This process yields hollow BNNPs with porous shell structures exhibiting a specific surface area of  $200.5 \text{ m}^2 \text{ g}^{-1}$  and a total pore volume of  $0.287 \text{ cm}^3 \text{ g}^{-1}$ , facilitating superior hydrogen accumulation [53].

The initial experimental synthesis of BN nanotubes via arc discharge was accomplished in 1995 by Chopra et al. [54]. The tight-binding theoretical model had predicted BN nanotube existence in 1993 by Rubio et al. [55], followed by Blase et al. the subsequent year, who employed *ab initio* pseudopotential methods to predict both single-walled and multi-walled BNNTs [56]. BN nanotubes are considered promising materials due to their enhanced Young's modulus ( $\sim 1.2 \text{ TPa}$ ), exceptional thermal stability, and chemical inertness. Defects such as vacancies and Stone–Wales defects commonly occur during nanostructure formation; consequently, defect engineering is widely employed to modify nanomaterial properties [57,58]. Several reports exist on BNNT synthesis. The selection of boron precursor, catalyst, temperature, heating regime, and duration is a critical factor in the synthesis process. The length and dimensions of BNNT may fluctuate based on these conditions. This section provides a concise overview of the synthesis methods and the characteristics of the resulting BNNTs. The precursors utilized in the synthesis of BNNT,

along with the mechanisms of formation, applications, and physical properties (such as diameters and lengths), are compiled in Table 2 [59].

**Table 2.** The literature outlines the reaction conditions, growth mechanisms, and applications of BNNT [59].

Precursor	T [°C]; t [h]	Substrate	Method	Growth Mechanism	Physical Properties	Modification	Application	Ref.
B, h-BN, NH <sub>3</sub>	<1100; 2	iron deposits alumina	ball milling (20 h), CVD	base-growth	40–100 nm diam., bamboo-like	–	–	[60]
	1200; 2				40–100 nm diam., cylindrical shape			
B:FeO:MgO (2:1:1), NH <sub>3</sub>	1200; 0.5	Si/SiO <sub>2</sub>	mechanic. mixed CVD	base-growth	30 nm diam., random direction, closed tip ends	–	–	[61]
	1300; 0.5			tip-growth	60 nm diam., random direction, closed tip ends			
	1400; 0.5			mixed-growth	10 nm diam., flower-like, closed tip ends			
B:FeO:MgO (1:1:1), NH <sub>3</sub>	1300; 0.5			tip- /base-growth	100–500 nm diam., closed tip ends			[62]
B:FeO:MgO (4:1:1), NH <sub>3</sub>	1300; 0.5			tip- /base-growth	50–150 nm diam., closed tip ends			
B <sub>2</sub> O <sub>3</sub> , CaB <sub>6</sub> , Mg, NH <sub>3</sub>	1150; 6	–	CVD	base-growth	150 nm diam., >10 µm length	–	–	
h-BN, N <sub>2</sub>	1250–1300; 10	–	ball milling (100 h), CVD	–	30–60 nm diam., cylindrical shape, 500 nm length	covalent with NH <sub>4</sub> HCO <sub>3</sub>	reinforced material for Al-matrix composite	[63]
B, FeO, MgO	1100–1700; 1	–	ball milling, CVD	metal catalytic growth	50–80 nm diam., up to 10 µm length, straight nanowires	noncoval. polyaniline/Pt/GO <sub>x</sub>	amper. glucose biosensor	[64]
B, iron particle, N <sub>2</sub>	1100; 15	Si/SiO <sub>2</sub>	ball milling (50 h), CVD	metal catalytic growth	50–200 nm diam., up to 1 mm length, bamboo-like	–	insulators for electromechanical systems	[65]
MWCNT, H <sub>3</sub> BO <sub>3</sub> , NH <sub>3</sub>	1300; 3	–	substitution	–	40–50 nm diam.	noncoval. trioctylam., tributylam., triphenyphos.	gel nanocomposite	[66]
B, Co(NO <sub>3</sub> ) <sub>2</sub> , N <sub>2</sub> , H <sub>2</sub>	1100; 0.5–3	stainless steel	ball milling, CVD	–	bamboo-like	–	superhydrophobic surface	[67]
B, N <sub>2</sub>	1200; 16	–	ball milling (150 h), CVD	–	20–50 nm diam. cylindrical, cylindrical capped by iron, bamboo-like	–	–	[68]
BH <sub>4</sub> , NH <sub>4</sub> Cl, N <sub>2</sub>	1200–1300; 5–10	–	CVD	–	10–30 nm diam., up to 5 µm length, bamboo-like	–	–	[69]
B, Fe <sub>2</sub> O <sub>3</sub> , NH <sub>3</sub>	1200–1300; 2.25	–	CVD	–	64–136 nm diam., bamboo-like	–	–	[70]
MWCNT, H <sub>3</sub> BO <sub>3</sub> , NH <sub>3</sub>	1080; 6	–	substitution	–	10–100 nm diam., 10 µm length	coval. PVA and HP-MEC	imp. mechanical performance of polymer	[71]

Table 2. Cont.

Precursor	T [°C]; t [h]	Substrate	Method	Growth Mechanism	Physical Properties	Modification	Application	Ref.
mmon. borane, ferrocn., N <sub>2</sub>	1450; 1	graphite crucible (graphite paper inner line)	CVD	(large diam. catalyst) vapor-liquid-solid (small diam. catalyst)	300 nm diam., 10 µm length, bamboo-like 15–200 nm diam., 100 µm length, cylindrical shape	–	–	[72]
B, Fe <sub>2</sub> O <sub>3</sub> , NH <sub>3</sub>	600; 1	–	CVD	–	20–60 nm diam. 2.5–4 nm diam.	–	hydrogen storage	[73]
B, Fe <sup>3+</sup> -MCM-41, NH <sub>3</sub>	600; 1	–	CVD	–	2.5–4 nm diam.	–	hydrogen storage	[73]
YB <sub>6</sub> , N <sub>2</sub> /Ar	–	–	arc discharge	mixed-growth	4–10 nm diam., 4–6 µm length, closed or open tip	–	–	[74]

In conclusion, due to its special structure and physicochemical characteristics, boron nitride (BN) remains one of the most promising materials for hydrogen storage. The diversity of its structural variations—from zero-dimensional nanoparticles to two-dimensional nanosheets—combined with high thermal stability, chemical inertness, and wide possibilities of surface modification, makes it attractive for both physical and chemical hydrogen sorption.

Recent studies, including both experimental work and DFT calculations, demonstrate the high capacity of BN for hydrogen storage, as well as its potential application in composites with LiBH<sub>4</sub> and other boron-based hydrides to destabilize and improve the reversibility of hydrogen storage processes [75–78].

Despite the existing limitations, progress in creating nanostructured forms of BN opens up new prospects in hydrogen energy and requires further in-depth research aimed at improving the efficiency and scalability of such solutions.

One area of interest is using h-BN as an additive to improve the hydrogen release (dehydrogenation) of lithium borohydride (LiBH<sub>4</sub>). The structural features of h-BN, such as the lone pair of electrons on nitrogen, defects in the crystal lattice, and interactions between B-H and B-N, contribute to destabilizing LiBH<sub>4</sub> [79].

Several studies have explored this application:

**Nanoporous h-BN:** Zhu et al. [79] used nanoporous h-BN to create a LiBH<sub>4</sub> composite that released 13.9 wt.% H<sub>2</sub> at 400 °C. However, the hydrogen storage capacity decreased over cycles, stabilizing at 7.6 wt.% H<sub>2</sub> after five cycles, due to the formation of Li<sub>2</sub>B<sub>12</sub>H<sub>12</sub> (leading to irreversibility) and Li<sub>x</sub>BN (important for rehydrogenation).

**Acid-treated h-BN:** Muthu et al. [80] employed acid-treated h-BN to prevent particle clumping during rehydrogenation. This composite released hydrogen between 110–150 °C and retained 85.7% of its initial capacity after four cycles.

Tu et al. [81] explored the synergistic influence of hexagonal boron nitride (h-BN) and niobium pentachloride (NbCl<sub>5</sub>) in destabilizing lithium borohydride (LiBH<sub>4</sub>), resulting in highly pure hydrogen liberation. NbCl<sub>5</sub> functioned as a catalyst, diminishing the dehydrogenation activation energy to 122 kJ/mol. Niobium hydride (NbH) particles, created in situ, acted as nucleation centers and decreased the solid–liquid interface during LiBH<sub>4</sub> breakdown.

Besides h-BN, other boron compounds can also destabilize LiBH<sub>4</sub>. For example, Li<sub>3</sub>BO<sub>3</sub> acts as a dehydrogenation catalyst by creating active sites, weakening Li-B bonds, promoting [BH<sub>4</sub>]<sup>−</sup> dissociation, and maintaining spatial proximity between Li, B, and

H atoms. Li et al. doped  $\text{LiBH}_4$  with  $\text{Nb}(\text{OEt})_5$ , which formed  $\text{Li}_3\text{BO}_3$  and  $\text{NbH}$ . This composite released 7.9 wt.%  $\text{H}_2$  within 20 min at 400 °C [82].

Li et al. [83] introduced niobium ethoxide ( $\text{Nb}(\text{OEt})_5$ ) as a dopant to  $\text{LiBH}_4$ , leading to the formation of  $\text{Li}_3\text{BO}_3$  and  $\text{NbH}$ . This composite yielded 7.9 wt.%  $\text{H}_2$  in 20 min at 400 °C. Following 30 sorption–desorption cycles, the material maintained 91% of its original capacity. The decline in reversibility was linked to the emergence of a stable  $\text{Li}_2\text{B}_{12}\text{H}_{12}$  phase.

Wu et al. [84] employed boric acid ( $\text{B}(\text{OH})_3$ ), where  $\text{O}-\text{H}_\delta^+$  and  $\text{B}-\text{H}_\delta^-$  interactions promoted  $\text{LiBH}_4$  dehydrogenation at reduced temperatures. The composite released 5.6 wt.%  $\text{H}_2$  below 180 °C, with minimal  $\text{H}_2\text{O}$  production. The main decomposition product identified was  $\text{LiB}_5\text{O}_9\text{H}_2$ . The dehydrogenation occurred swiftly, releasing 4.5 wt.%  $\text{H}_2$  within 2 min at 180 °C. However, the exothermic nature of the reaction restricted its reversibility.

Eutectic blends of  $\text{LiBH}_4$  with different metal borohydrides ( $\text{MBH}_4$ ) have been widely researched. These blends exhibit lower melting points compared to their individual constituents, while preserving significant theoretical hydrogen storage capacities, around 10 wt.%  $\text{H}_2$ . The dehydrogenation temperature of these blends is primarily dictated by the characteristics of the additional component, rather than their melting temperatures [85].

To investigate the destabilization of  $\text{LiBH}_4$ , several borohydrides, such as  $\text{La}(\text{BH}_4)_3$ ,  $\text{Er}(\text{BH}_4)_3$ ,  $\text{KBH}_4$ , and  $\text{NaBH}_4$ , have been analyzed [86–88]. However, these eutectic combinations, when in the bulk state, did not demonstrate sufficient destabilization of  $\text{LiBH}_4$ . Hydrogen liberation usually took place at temperatures exceeding 300 °C, with some instances surpassing 500 °C, rendering them unsuitable for hydrogen storage purposes.

In another study [89], boron nitride nanosheets modified with oxygen, synthesized using the sol-gel technique, were analyzed. This material demonstrated a hydrogen storage capability of 5.7 wt.% at ambient temperature and a pressure of 5 MPa. Notably, each  $3 \times 3$  supercell within the BN monolayer could accommodate up to six  $\text{H}_2$  molecules. Theoretical modeling suggests that the enhanced hydrogen storage performance is likely due to the introduction of oxygen into the BN nanosheets. This doping process reduces the distance between hydrogen molecules and oxygen atoms during adsorption, compared to pristine BN. The two most important are shown in Figure 2 the low temperature phase of  $\text{LiBH}_4$ , known as orthorhombic- $\text{LiBH}_4$  (*o*- $\text{LiBH}_4$ ), which transforms into high temperature hexagonal- $\text{LiBH}_4$  (*h*- $\text{LiBH}_4$ ) phase at  $\sim 388$  K. At ambient pressures, *h*- $\text{LiBH}_4$  exists in SG  $P6_3mc$  (Figure 3) [89].

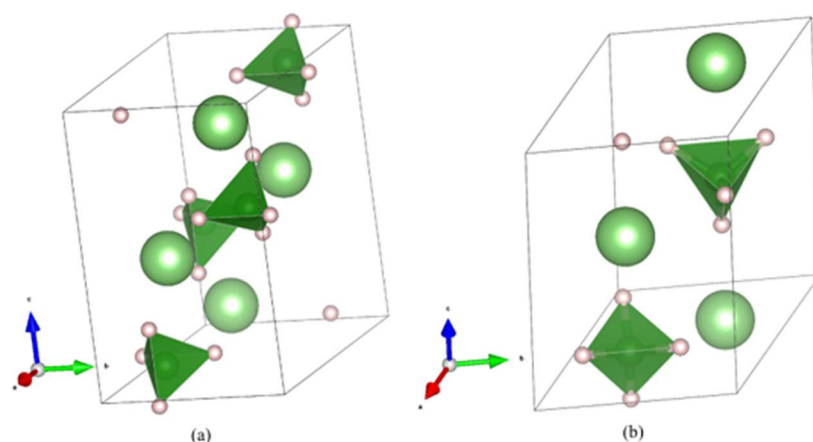


**Figure 2.** (Color online). (a) The room temperature, orthorhombic- $\text{LiBH}_4$  (*o*- $\text{LiBH}_4$ ), transforms into (b) hexagonal- $\text{LiBH}_4$  (*h*- $\text{LiBH}_4$ ) at  $\sim 388$  K. At ambient pressures, the *o*- and *h*- $\text{LiBH}_4$  exist in space groups  $Pnma$  and  $P6_3mc$ . Li = green, hydrogen = whitish, boron = inside green tetrahedral [89].

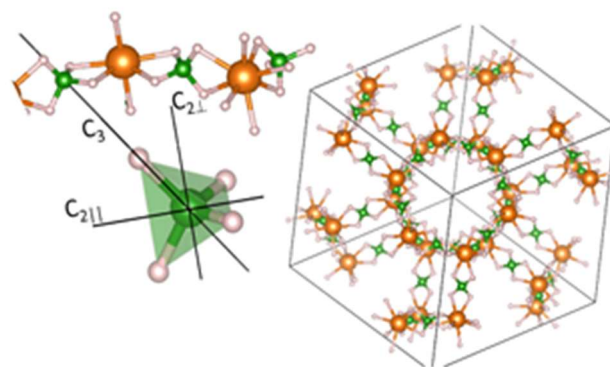


**Figure 3.** The left image shows three  $[BH_4]$  tetrahedra in their respective Mg setting and a magnification of one tetrahedra with its rotational axes.  $C_3$  is the 3-fold  $120^\circ$  axis, and  $C_{2\parallel}$  and  $C_{2\perp}$  are the 2-fold  $180^\circ$  axis. The right image shows the crystal structure of  $\gamma$ - $Mg(BH_4)_2$  with one interpenetrating channel. Spheres in orange: Mg-, green: B-, and grey: H-atoms [89].

Additional research [90] focused on evaluating the structural integrity of metal-doped BN systems and identifying preferred metal adsorption locations on the BN layers. An examination of sodium-doped BN layers revealed that the electric field formed between positively charged sodium and negatively charged nitrogen plays a crucial role in strengthening the bond between hydrogen and the complex. This enhancement occurs through hydrogen polarization. Consequently, the sodium-doped layer achieved a hydrogen storage capacity of approximately 5.84 wt.%.

Magnesium and its alloys have recently attracted increasing attention as promising hydrogen storage materials due to their significant reversible capacity (up to 7.6 wt.%) and affordable cost. Among the hydrides used in hydrogen energy, magnesium hydride ( $MgH_2$ ) stands out for its high energy capacity—up to 9 MJ/kg Mg—and its ability to undergo reversible hydrogenation/dehydrogenation reactions [91].

Figure 4 shows various dehydrogenation processes (highlighted in blue) and rehydrogenation reactions (highlighted in red) [92].

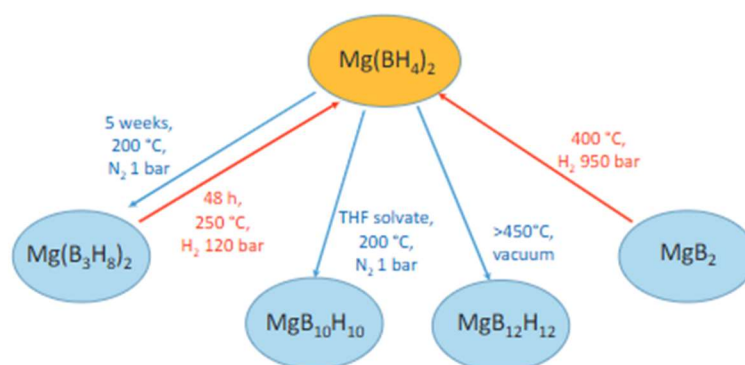


**Figure 4.** Selected hydrogenation (in red) and dehydrogenation (in blue) reactions with  $Mg(BH_4)_2$  [92].

Despite its advantages, the use of  $MgH_2$  is limited by a number of important factors: Challenging operating conditions: high temperatures (about  $300^\circ C$ ) and pressures (5–10 MPa) are required for effective hydrogenation.

Kinetic limitations: Slow kinetics of reversible hydrogen binding processes, which complicates the absorption and release of hydrogen.

Activation issues: High energy barrier for  $H_2$  dissociation on Mg surface, resulting in poor chemisorption.

Passivation layer formation: The forming  $\text{MgH}_2$  layer impedes diffusion, making further hydrogenation difficult.

Oxygen sensitivity: Surface oxidation upon contact with  $\text{O}_2$  reduces the rate of hydrogen uptake.

Cycling degradation: Gradual loss of capacity over repeated hydrogenation / dehydrogenation cycles [92].

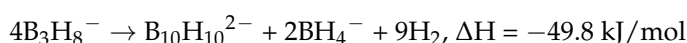
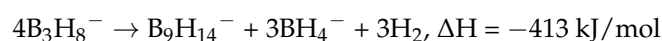
To improve the performance of hydrogen storage systems, the interaction of magnesium hydrides with boranes is studied. It was found that the thermal decomposition of  $\text{Mg}(\text{BH}_4)_2$  in a vacuum is likely to result in the formation of the intermediate compound  $\text{Mg}(\text{B}_3\text{H}_8)_2$ . Similarly, heating  $\text{Y}(\text{BH}_4)_3$  under a hydrogen pressure of 1–10 bar allows one to obtain the compound  $\text{Y}(\text{B}_3\text{H}_8)_3$ . Various methods for the synthesis and transformation of the  $\text{B}_3\text{H}_8^-$  anion are described in the literature, including the following:

Reactions with diborane under strong reduction conditions, leading to the formation of intermediate anions  $\text{B}_2\text{H}_6^{2-}$  and  $\text{BH}_6^{2-}$ , which are confirmed by NMR spectroscopy [93–95]. Interaction of potassium with THF  $\text{BH}_3$ , resulting in the formation of  $\text{B}_3\text{H}_8^-$  and  $\text{BH}_4^-$ .

Reactions of  $\text{BH}_4^-$  with  $\text{B}_2\text{H}_6$ , yielding  $\text{B}_3\text{H}_8^-$  and releasing hydrogen.

Synthesis of  $\text{B}_3\text{H}_8^-$  from  $\text{BH}_4^-$  and  $\text{CH}_2\text{Cl}_2$  at elevated temperatures.

The resulting  $\text{B}_3\text{H}_8^-$  can further participate in reactions leading to the formation of more complex borane clusters ( $\text{B}_9$ ,  $\text{B}_{10}$ ,  $\text{B}_{12}$ , etc.):



These reactions are thermodynamically favorable and are accompanied by a significant entropy increase, particularly at elevated temperatures. The concurrent formation of  $\text{BH}_4^-$  provides an additional thermodynamic driving force for these transformations (Figure 5) [96].

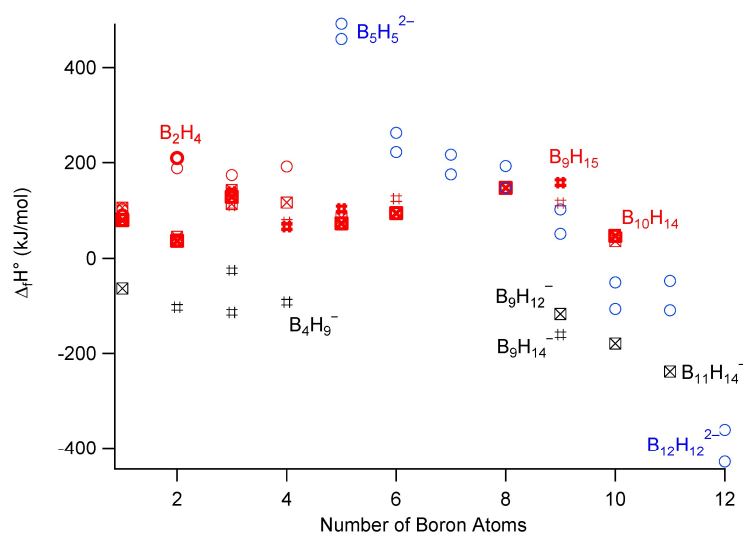


**Figure 5.** Experimental (bold) and theoretical formation enthalpy values for neutral (red), monoanionic (black), and dianionic (blue) species. *Closo* species, circles; *nido*, #; *arachno*, crossed squares. Data from [97–102]. For *closo* ions  $\text{B}_n\text{H}_n^{2-}$ , data (blue circles) from two different studies reveal systematic differences. All monoanionic species (in black) have negative formation enthalpies, while all neutral boranes (in red) have positive formation enthalpies [96].

Heating  $\text{Mg}(\text{B}_3\text{H}_8)_2$  combined with  $4\text{MgH}_2$ , whether or not hydrogen is present, results in a conversion of up to 88% back to  $\text{Mg}(\text{BH}_4)_2$ , along with the formation of some

MgB<sub>12</sub>H<sub>12</sub>. This process facilitates the development of closed synthesis/decomposition cycles for hydrides, aiming to improve the effectiveness of hydrogen storage systems. The B<sub>3</sub>H<sub>8</sub><sup>−</sup> ion can also serve as a building block for producing multi-component solid-state ionic conductors. For example, highly ionically conductive materials such as Na<sub>4</sub>(B<sub>10</sub>H<sub>10</sub>)(B<sub>12</sub>H<sub>12</sub>) can be synthesized. This synthesis pathway involves transforming NaBH<sub>4</sub> into (Et<sub>4</sub>N)BH<sub>4</sub>, followed by a reaction with CH<sub>2</sub>Cl<sub>2</sub>, a thermal transformation into toluene, and exchange reactions using sodium tetraphenylborate [103–105].

### 3. Summary of Hydrogen Storage and Release in h-BN-Based Materials

The current body of research reveals a notable lack of empirical information concerning the hydrogenation and dehydrogenation mechanisms of hexagonal boron nitride (h-BN). Most studies primarily employ computational modeling. Further experimental investigations, concentrating on the release of hydrogen from h-BN-based compounds, are of significant importance. A considerable number of publications neglect to examine the reusability of BN materials after undergoing dehydrogenation/desorption, or to elucidate the impact of hydrogen storage and release at the relevant temperatures on their characteristics [106,107].

Hydrogen adsorption phenomena have been explored extensively on various nanotube types and their modified versions over the last ten years. Different approaches have been used to explore hydrogen molecule adsorption on boron nitride nanotubes (BNNTs), including those functionalized with metals [108] like Rh, Ni, and Pd. The adsorption of hydrogen molecules on Al-doped BNNTs (5,0) and (3,3) has also been examined, with data given on the quantity of adsorbed hydrogen molecules and mean adsorption energies [109].

Multiple studies have established that metallic magnesium's surface is critical for hydrogen absorption, promoting the separation of H<sub>2</sub> molecules and facilitating hydrogen atom diffusion into the material's core (Table 3). Ball milling, which involves mechanically processing magnesium or its hydride using high-energy techniques, represents cutting-edge methods for improving and accelerating hydrogenation–dehydrogenation processes. This approach is widely used to enhance the surface properties of metal hydrides [110].

**Table 3.** Hydrogen absorption/desorption properties of selected magnesium-based metal hydrides and their alloys [110].

Material	Method	Temperature (°C)	Pressure (MPa)	Kinetic (min)	Cyclical Stability	Max.% (mas.) H <sub>2</sub>	Ref.
Mg/MgH <sub>2</sub> -5% (mac.) Ni	Wet chemical method	T <sub>abs.</sub> 230–370	P <sub>abs.</sub> and P <sub>des.</sub> 0.4–0.14	t <sub>abs.</sub> 90	800 cycles, stable	6.0	[111]
MgH <sub>2</sub> -0.2% (mol.) Cr <sub>2</sub> O <sub>3</sub>	BM	T <sub>abs.</sub> and T <sub>des.</sub> 300	P <sub>abs.</sub> and P <sub>des.</sub> 0.1–0.2	t <sub>abs.</sub> 6 t <sub>des.</sub> 10–35	1000 cycles, stable	6.40	[112]
MgH <sub>2</sub>	BM	T <sub>abs.</sub> 300 and T <sub>des.</sub> 350	P <sub>abs.</sub> 0.3–1.0 P <sub>des.</sub> 0.015	t <sub>des.</sub> 12.5 t <sub>des.</sub> 50 t <sub>abs.</sub> 420	-	7.0	[113]
MgH <sub>2</sub> -1% (at.) Al	BM benzene or hexane	T <sub>bs.</sub> 180 T <sub>des.</sub> 335–347	P <sub>abs.</sub> 0.06		-	7.30	[114]

DFT was utilized to explore how structural defects and substitutional doping affect the ability of BNNTs to adsorb hydrogen. The results indicated that the binding energy significantly increased when compared to the ideal BN structure. It was also shown that

the projected desorption temperature is approximately 123 K, and hydrogen diffuses more slowly in BNNTs with smaller diameters than in those with larger diameters. The binding energy of BN nanotubes is also about 40% higher than that of carbon nanotubes [115]. The impact of Pt modification on BN nanotubes, which results in a high average adsorption energy of hydrogen molecules at  $-0.365$  eV, was examined using DFT simulations in [116].

The connection between the Pt atom and the BN nanotube was shown to be weakened by the adsorptive hydrogen molecule. The formation of a Pt dimer after two Pt atoms are doped onto a BN nanotube weakens the Pt-BN connection and lowers the adsorption energy of hydrogen molecules on the Pt dimer. A theoretical study of the structure, stability, and hydrogen storage capabilities of hydrogenated h-BN sheets doped with lithium was also carried out in [117]. Li atoms on h-BN sheets were shown to act as binding sites, absorbing up to 6 weight percent hydrogen at lower temperatures ( $<198$  K). Ab initio modeling suggests a hydrogen desorption temperature of  $\sim 398$  K. In addition to pure lithium, its compounds have also been shown to be effective modifiers for increasing the hydrogen storage capacity of h-BN. The calculated gravimetric hydrogen density of  $2(\text{OLi}_3)$ -decorated h-BN for storing  $\text{H}_2$  molecules can reach 9.67 wt.% [118].  $-0.175$  eV, the average adsorption energy per  $\text{H}_2$  molecule, is the ideal window for reversible uptake-release at room temperature.

Composites of Ti powder that had been mechanically milled with h-BN at a mass ratio of 1:1 achieved a hydrogen adsorption capacity of 4.2 wt.%. The observed value is consistent with the theoretical calculations for hydrogen uptake by Ti, indicating that Ti is essential for hydrogen absorption in the analyzed mixture [119]. DFT calculations were used in a different study (Chen et al., 2012) [120] to investigate the adsorption of transition metals, including Sc, Ti, V, Cr, Mn, Fe, Co, and Ni, on carbon-doped h-BN sheets and the  $\text{B}_{12}\text{N}_{12}$  cage. Sc, V, Cr, and Mn exhibited favorable energetics for dispersion on the sheet and CN-BN cage, with a hydrogen absorption capacity of up to 6 wt.%. It has been demonstrated that carbon dopants in h-BN can function as potential traps for metal atoms, preventing their clustering [120].

A new method for hydrogen storage utilizing pure h-BN bubbles, which are emerging convex structures on the h-BN surface, through plasma treatment has been proposed [121]. To identify the type of gas trapped inside the h-BN bubbles, low-temperature atomic force microscopy (AFM) measurements were conducted to monitor how the bubbles responded to temperature changes. This experiment was inspired by recent research on bubble structures in bulk transition metal dichalcogenides.

Figure 6a presents an optical image of bubbles on an h-BN flake. After transferring the sample into a vacuum chamber equipped with AFM, it was gradually cooled. Topographic AFM images of the same region at 34 K and 33 K are shown in Figure 6b. It is evident that the bubbles are inflated with gas at 34 K but collapse at 33 K. As illustrated in Figure 6c, height profiles taken along the dashed lines in Figure 6b demonstrate that the bubble is visible at 34 K but disappears at 33 K.

This inflation–deflation behavior was reversible and reproducible upon heating and cooling. The highest temperature at which the bubbles flattened was defined as the transition temperature ( $T_{\text{transition}}$ ). A histogram was then constructed (Figure 6d), showing the distribution of  $T_{\text{transition}}$  values with 1 K intervals.

The  $T_{\text{transition}}$  values followed a Gaussian distribution, with an average of  $33.2 \pm 3.9$  K, which closely matches the known transition temperature of hydrogen (33.18 K). This strongly suggests that the gas trapped inside the h-BN bubbles is hydrogen [121].

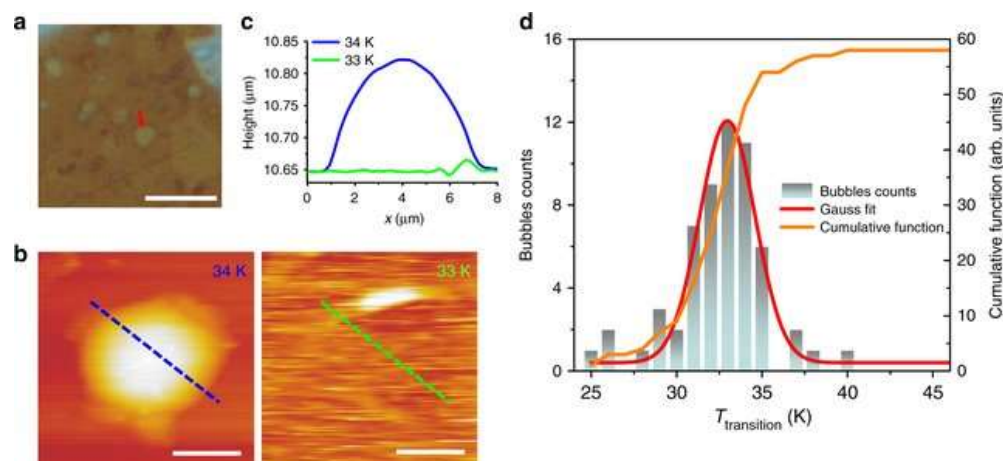


**Figure 6.** Swelling and deflating processes of the h-BN bubbles containing hydrogen. (a) An optical image of bubbles on an h-BN flake, taken under ambient conditions, scale bar: 20  $\mu\text{m}$ . (b) Topographic AFM image of a bubble pointed out by an arrow in (a) was measured at 34 and 33 K, respectively, scale bars: 3  $\mu\text{m}$ . (c) The height profiles of the line-scan at the same place (indicated by dashed lines in (b)) where the bubble remains at  $\sim 34$  K and disappears at  $\sim 33$  K. (d) Histogram of the transition temperature ( $T_{\text{transition}}$ ) at which bubbles collapse. The red line is a Gaussian fit to the data. The yellow line is the histogram cumulative function (right axis) [121].

These bubble structures, created from methane plasma, exhibit diameters between 2 and 4  $\mu\text{m}$  and heights reaching up to 8.5 nm. The stability of hydrogen bubbles, influenced by geometric evolution, indicates that the diameters of all bubbles typically maintain stability for approximately 30 weeks in ambient conditions. This approach shows potential for hydrogen preservation; however, the extraction aspect is still not addressed.

A comparison of various BN-based materials in terms of their hydrogen storage capacity is presented in Table 4 [122].

**Table 4.** Comparison of BN-based materials for hydrogen storage [122].

Storage Ability, wt%	Morphology	Material's Features	Storing Conditions		References
			P, MPa	T, K	
<b>Experimental data</b>					
2.9	Nanofibres	30–100 nm width and several $\mu\text{m}$ length	10	293	[123]
1.8	Multifalled nanotubes		10	293	[124]
2.5	Flower-type nanostructures	Specific surface area about $180 \text{ m}^2 \text{ g}^{-1}$	10	298	[125]
2.6	Bamboo-like nanotubes	10–80 nm width and $> \mu\text{m}$ length	10	293	[126]
3.0	Bamboo-like nanotubes	Specific surface area about $180 \text{ m}^2 \text{ g}^{-1}$	10	298	[127]
0.2	Bulk powder	-	10	293	[123]
0.1	Bulk powder	-	6	293	[123]
2.6	Nanostructured milled powder	Fine-milled (80 h)	1	293	[126]
4.2	Collapsed nanotubes	Catalyzed by the Pt	10	293	[127]

Table 4. Cont.

Storage Ability, wt%	Morphology	Material's Features	Storing Conditions		References
			P, MPa	T, K	
5.7	o-doped	Nanosheets with 2–6 atomic layers	5	293	[127]
2.57	Porous microsponge	Ultrahigh surface area up to 1900 m <sup>2</sup> g <sup>-1</sup>	1	77	[128]
5.6	Micro/meso-porous	High surface area of 1.687 m <sup>2</sup> g <sup>-1</sup> , pore volume of 0.99 cm <sup>3</sup> g <sup>-1</sup> , rich structural defects	3	298	[129]
2.3	Porous microbelts	High surface area up to 1.488 m <sup>2</sup> g <sup>-1</sup>	1	77	[130]
<b>Theoretical modeling data</b>					
1.5	Pristine	-	5	293	[131]
1.9	o-doped	Interlayer distance 7–7.5 Å	5	293	[132]
5.5	o-doped	-		N/a	[126]
2.81	Pt-doped sheets	-		N/a	[131]
4.82	Pt-doped sheets	-		N/a	[131]
6.33	C-doped nanosheets modified with Ti	-	0.5	298	[132]
5.1	Porous	Ultrahigh surface area 3.260 m <sup>2</sup> g <sup>-1</sup>		N/a	[133]
7.5	Li-decorated porous	One-side decoration		N/a	[133]
8.65	Li-doped nanosheets	Distance between sheets 8.3 Å	0.1	300	[131]
9.67	h-BN monolayer	2(Oli <sub>3</sub> )-decorated		N/a	[134]
3.4	h-BN bilayer	Sorption in the interlayer spacing		N/a	[135]
6.7	h-BN bilayer	Sorption on the h-BN surface		N/a	[136]
3.86	eh-BN	Expanded h-BN	20	243	[137]
11.21	O-B <sub>2</sub> N <sub>2</sub> monolayer	Decorated by Ti atoms		-	[138]

The ability of materials to store hydrogen is strongly influenced by their specific surface area and, consequently, their structural arrangement. A larger specific surface area encourages the development of imperfect structures, featuring multiple layers and exposed edges on the surface. Among high-surface-area forms of h-BN nanostructures, nanotubes are particularly promising for hydrogen storage at room temperature. Research indicates that chemisorption is generally more prevalent than physisorption in BN nanotubes. This results in a requirement for greater energy inputs to remove hydrogen (during the dehydrogenation process).

BN nanofibers, with diameters between 30 and 100 nm and lengths spanning several micrometers, exhibit a hydrogen storage capacity of roughly 2.9 wt.% at 293 K and 100 bar. However, it is worth noting that only a small fraction of the stored hydrogen, about 20 wt.%, is released at room temperature, representing the physisorbed portion. To release the chemisorbed hydrogen, a temperature of 573 K is needed. Similar findings were

reported, where bamboo-like BN nanotubes retained approximately 70% of the stored hydrogen after pressure reduction, suggesting chemisorption as the predominant mechanism. Complete release of adsorbed hydrogen only occurred upon heating the sample to 573 K. In subsequent cycles, the hydrogen uptake capacity remained consistent, indicating reversible adsorption–desorption processes. This suggests that imperfect structures enhance chemical interactions with hydrogen, leading to the creation of stable bonds.

According to Ma et al. (2002a) [124], hydrogen adsorption on multi-walled BN nanotubes (specific surface area: 150 m<sup>2</sup>/g) and bamboo-like BN nanotubes (specific surface area: 210 m<sup>2</sup>/g) at 293 K and 100 bar reached 1.8 wt.% and 2.6 wt.%, respectively. Moreover, experimental studies show that the hydrogen storage potential in h-BN nanostructures increases with hydrogen pressure. For instance, straight-walled BN nanotubes (specific surface area: 210 m<sup>2</sup>/g) exhibit an enhanced capacity of 2.7 wt.% under the same conditions, while flower-like BN nanostructures (specific surface area: 180 m<sup>2</sup>/g) demonstrate a maximum hydrogen storage capacity of 2.5 wt.% at around 100 bar. The bamboo-type nanotubes, featuring the highest specific surface area (230 m<sup>2</sup>/g), also exhibit the highest hydrogen uptake (3.0%).

Additionally, a proposed mechanism allows for the regeneration of triflic acid during operation, ensuring gradual hydrogen release over time. In comparison, Pt-catalyzed collapsed BN nanotubes release 5% of adsorbed hydrogen in the 353–413 K range and the remaining 95% in the 573–723 K range [125].

The researchers Tang et al. (2002) [127] investigated the hydrogen storage potential of various BN configurations at 10 MPa and room temperature. Their findings highlighted that BN nanotubes, when collapsed, exhibit a significantly improved hydrogen adsorption capacity compared to conventional multi-walled nanotubes. This enhancement was attributed to an increased density of dangling bonds and a substantial elevation in specific surface area, which rose from 254.2 m<sup>2</sup>/g to 789.1 m<sup>2</sup>/g. The observed hydrogen uptake ranged from 0.9 to 4.2 wt.%. Further studies [128] showed that approximately 89% of the hydrogen stored in oxygen-doped h-BN nanosheets could be released at room temperature simply by reducing the pressure to ambient conditions. Furthermore, the hydrogen absorption capacity experienced only a slight decrease, from 5.7 to 4.79 wt.%, over 15 cycles of adsorption and desorption.

The capacity of nanomaterials for hydrogen sorption is significantly affected by chemical functionalization. Oxygen-doped h-BN nanosheets (2–6 layers), created through the sol-gel method [130], can store up to 5.7 wt.% hydrogen at room temperature and 5 MPa. This material exhibited remarkable cyclic stability, maintaining its performance over 15 hydrogen uptake and release cycles. Another study (Zhang et al., 2015) [134] underscored the potential of porous boron nitride (p-BN) as a promising structure for hydrogen storage.

Theoretical investigations using first-principles calculations suggested that pristine h-BN bilayers could function as hydrogen storage materials, providing a maximum capacity of 3.4 wt.% with desorption temperatures ranging from 139 K to 279 K, contingent on the quantity of adsorbed H<sub>2</sub> molecules [136]. DFT calculations indicated that a Ti-decorated orthorhombic diboron dinitride (o-B<sub>2</sub>N<sub>2</sub>) monolayer could attain a storage capacity of 11.21 wt.% with a 396 K desorption temperature [137].

Releasing chemisorbed hydrogen (including hydrogen from hydrogenated functional groups) from BN-based materials often demands additional energy due to the strong bonds involved. For instance, nanostructured h-BN powder, capable of storing 2.6 wt.% hydrogen, requires heating to 570 K for complete release [138]. Chemisorbed hydrogen within BN nanotubes typically necessitates temperatures exceeding 623 K for release. However, triflic

acid can catalyze this process, facilitating efficient dehydrogenation at modestly elevated temperatures (313–323 K) [139–142].

A novel structure,  $B_{20}N_{24}$  [143], designed via the CALYPSO code, presents itself as a potential hydrogen storage candidate, with simulations indicating a 6.8 wt.% storage capacity corresponding to 19 adsorbed  $H_2$  molecules. First-principles quantum-chemical calculations reveal that C-doped p-BN can achieve a maximum hydrogen uptake of 5.1 wt.%, while Li-doped p-BN can adsorb up to 7.5 wt.% hydrogen. Similar analyses apply to materials like Li-functionalized  $BC_2N$  monolayers and boron/carbon-doped structures. Furthermore, dispersion-corrected semi-empirical methods suggest that  $B_{96}N_{96}$  nanocages can exhibit the highest hydrogen uptake at 12.01 wt.%. Notably, theoretically designed TM-fullerenes  $B_{24}N_{24}$  (TM = Sc, Ti) demonstrate gravimetric hydrogen densities of 7.74 wt.% ( $Sc_6B_{24}N_{24}$ ) and 7.50 wt.% ( $Ti_6B_{24}N_{24}$ ), with hydrogen release temperatures falling within the 243–408 K range [144–146]. These combined theoretical and experimental results provide optimism for the development of effective hydrogen storage devices based on nanostructured h-BN.

The mechanisms of hydrogen uptake and release in hexagonal boron nitride (h-BN) are still not fully understood, with current research heavily dependent on computational simulations [147]. There is a significant lack of experimental evidence concerning the ability of h-BN to be reused following hydrogen liberation, as well as data on how the material's characteristics change after dehydrogenation. Recent work has focused on how hydrogen is adsorbed onto boron nitride nanotubes (BNNTs) and their altered versions, like those with added metals or aluminum. To boost hydrogen adsorption, metal hydrides like magnesium-based compounds have been used, with mechanical milling techniques improving the speed and amount of hydrogen absorbed.

Computational studies employing DFT have shown that adding metals, such as platinum (Pt), can greatly improve how well hydrogen sticks to BN structures. It has been reported that adding lithium can raise the hydrogen storage capability of h-BN to as much as 9.67 wt.%. Additionally, experimental research indicates that hydrogen storage capacities differ depending on the shape of the h-BN, with bamboo-like BN nanotubes exhibiting the highest capacity (3.0 wt.% at 298 K), but hydrogen release necessitates temperatures close to 573 K.

New materials, including doped h-BN and  $B_{20}N_{24}$  clusters, have demonstrated considerable potential. Theoretical models suggest effective hydrogen storage and release between 243 and 408 K. These results, drawn from both theoretical calculations and experimental observations, offer a solid base for the ongoing development of nanostructured h-BN as a potential advanced material for storing hydrogen.

#### 4. Conclusions

Current scholarly investigations suggest that boron nitrides stand out as particularly appealing substances for hydrogen storage applications. Both computer simulations and real-world tests highlight the considerable promise of hydrogen storage systems built around h-BN materials. According to these findings, strategies for boosting the hydrogen absorption capabilities of h-BN materials involve enlarging the effective surface area, creating structural imperfections to change the crystal structure, and possibly changing the distance between layers. Additional methods include adding other elements to BN and creating metal-based coatings on the surface through functionalization (for example, using Ti, Li, etc.).

Nevertheless, several key issues have slowed the advancement of BN as a material for hydrogen storage. First, major scientific interest in BN is a fairly recent phenomenon, with initial research appearing in the early 2000s. Its development has been slow compared

to materials found later. Secondly, there is significantly more theoretical work (based on computational methods) than experimental research. These theoretical studies have improved our understanding of how BN absorbs hydrogen and have suggested different ways to improve it. However, the absence of experimental confirmation has made it harder to use BN as a hydride in practice.

Therefore, the most effective way to create high-performing hydrogen storage systems based on BN is to conduct a series of experiments that focus on layer-by-layer ball milling. This method results in a bigger specific surface area, a microstructure with smaller grains, many flaws (both on the surface and inside), the creation of phase boundaries, and a porous surface structure with numerous active sites for hydrogen absorption and desorption. These changes can greatly improve how fast hydrogenation happens and its thermodynamic features while keeping the hydrogen storage capacity almost the same.

Moreover, it is necessary to continue in-depth studies on how hydrogen is released and how well BN-based materials can be recycled after many cycles of adding and removing hydrogen.

**Author Contributions:** Conceptualization, Y.K. and S.K.; validation, N.M., A.U. and A.K.; formal analysis, L.B.; investigation, S.K.; resources, Y.K. and S.K.; data curation, Y.K., S.K. and L.B.; writing—original draft preparation, D.B. and S.K.; writing—review and editing, Y.K. and S.K.; visualization, D.B., A.U. and A.K.; supervision, N.M.; project administration, R.N.; funding acquisition, R.N. and N.M. All authors have read and agreed to the published version of the manuscript.

**Funding:** This research has been funded by the Science Committee of the Ministry of Science and Higher Education of the Republic of Kazakhstan (Grant No. AP22784686).

**Data Availability Statement:** The raw data supporting the conclusions of this article will be made available by the authors on request.

**Conflicts of Interest:** The authors declare no conflicts of interest.

## References

1. Özdoğan, K.; Berber, S. Optimizing the hydrogen storage in boron nitride nanotubes by defect engineering. *Int. J. Hydrogen Energy* **2009**, *34*, 5213–5217. [\[CrossRef\]](#)
2. Portehault, D.; Giordano, C.; Gervais, C.; Senkovska, I.; Kaskel, S.; Sanchez, C.; Antonietti, M. High-Surface-Area Nanoporous Boron Carbon Nitrides for Hydrogen Storage. *Adv. Funct. Mater.* **2010**, *20*, 1827–1833. [\[CrossRef\]](#)
3. Skakov, M.; Batyrbekov, E.; Sokolov, I.; Miniyazov, A.; Tulenbergenov, T.; Sapataev, Y.; Orazgaliyev, N.; Bukina, O.; Zhanbolatova, G.; Kozhakhmetov, Y. Influence of Hydrogen Plasma on the Surface Structure of Beryllium. *Materials* **2022**, *15*, 6340. [\[CrossRef\]](#)
4. Skakov, M.; Kozhakhmetov, Y.; Mukhamedova, N.; Miniyazov, A.; Sokolov, I.; Urkunbay, A.; Zhanbolatova, G.; Tulenbergenov, T. Effect of a High-Temperature Treatment on Structural-Phase State and Mechanical Properties of IMC of the Ti-25Al-25Nb at.% System. *Materials* **2022**, *15*, 5560. [\[CrossRef\]](#) [\[PubMed\]](#)
5. Moussa, G.; Moury, R.; Demirci, U.; Miele, P. Boron-based hydrides for chemical hydrogen storage. *Int. J. Hydrogen Energy* **2013**, *38*, 14007–14023. [\[CrossRef\]](#)
6. Umegaki, T.; Yan, J.M.; Zhang, X.B.; Shioyama, H.; Kuriyama, N.; Xu, Q. Hydrogen storage in boron nitride nanotubes: A first-principles study. *Int. J. Hydrogen Energy* **2009**, *34*, 2303–2311. [\[CrossRef\]](#)
7. Blinov, D.V. Issledovanie Teplovykh Protsesov v Sistemakh Tverdogaznogo Akkumulirovaniya i Ochistki Vodoroda. Ph.D. Thesis, Moscow State Technical University, Moscow, Russia, 2016.
8. Matsuo, M.; Nakamori, Y.; Orimo, S.; Maekawa, H.; Takamura, H. Lithium superionic conduction in lithium borohydride accompanied by structural transition. *Appl. Phys. Lett.* **2007**, *91*, 224103. [\[CrossRef\]](#)
9. Gunathilake, C.; Soliman, I.; Panthi, D.; Tandler, P.; Fatani, O.; Ghulamullah, N.A.; Marasinghe, D.; Farhath, M.; Madhujith, T.; Conrad, K.; et al. A Comprehensive Review on Hydrogen Production, Storage, and Applications. *Chem. Soc. Rev.* **2024**, *53*, 10900–10969. [\[CrossRef\]](#) [\[PubMed\]](#)
10. Scarpati, D.; Orecchini, F.; Guida, M. Metal Hydrides for Hydrogen Storage: Current Status and Future Perspective. *J. Energy Storage* **2024**, *72*, 108587. [\[CrossRef\]](#)

11. Mahmoud, H.A.; Zhang, X.; Li, J. Porous Carbon Materials for Hydrogen Storage: Strategies and Recent Developments. *RSC Adv.* **2024**, *14*, 2154–2170. [[CrossRef](#)]
12. Elyasi, R.; Heidari, R.; Ghasemi, M. Biomass-Derived Nanoporous Carbon Materials for Solid-State Hydrogen Storage: Advances and Outlook. *Int. J. Hydrogen Energy* **2024**, *49*, 5678–5692. [[CrossRef](#)]
13. Soni, S.; Pathak, A.K.; Singhal, R. Carbon-Based Materials for Hydrogen Storage: A Critical Review. *Carbon. Energy* **2021**, *3*, 700–724. [[CrossRef](#)]
14. Sutton, A.; Sutton, A.G.; Mardel, J.I.; Hill, M.R. Metal-Organic Frameworks (MOFs) as Hydrogen Storage Materials at Near-Ambient Temperature. *Chem. Eur. J.* **2024**, *30*, e202400717. [[CrossRef](#)] [[PubMed](#)]
15. Wang, J.; Chen, Y.; Yuan, L.; Zhang, M.; Zhang, C. Scandium Decoration of Boron Doped Porous Graphene for High-Capacity Hydrogen Storage. *Molecules* **2019**, *24*, 2382. [[CrossRef](#)] [[PubMed](#)]
16. Roy, S.; Zhang, X.; Puthirath, A.B.; Meiyazhagan, A.; Bhattacharyya, S.; Rahman, M.M.; Babu, G.; Susarla, S.; Saju, S.K.; Tran, M.K.; et al. Structure, Properties and Applications of Two-Dimensional Hexagonal Boron Nitride. *Adv. Mater.* **2021**, *33*, 2101589. [[CrossRef](#)] [[PubMed](#)]
17. Verdal, N.; Her, J.-H.; Stavila, V.; Soloninin, A.V.; Babanova, O.A.; Skripov, A.V.; Udovic, T.J.; Rush, J.J. Complex high-temperature phase transitions in  $\text{Li}_2\text{B}_{12}\text{H}_{12}$  and  $\text{Na}_2\text{B}_{12}\text{H}_{12}$ . *J. Solid. State Chem.* **2014**, *212*, 81–91. [[CrossRef](#)]
18. IEA. *Emissions from Oil and Gas Operations in Net Zero Transitions: A World Energy Outlook Special Report for COP28*; IEA: Paris, France, 2023.
19. Jena, P. Materials for Hydrogen Storage: Past, Present, and Future. *J. Phys. Chem. Lett.* **2011**, *2*, 206–211. [[CrossRef](#)]
20. Gulino, V.; Brighi, M.; Dematteis, E.M.; Murgia, F.; Nervi, C.; Cerny, R.; Baricco, M. Phase Stability and Fast Ion Conductivity in the Hexagonal  $\text{LiBH}_4\text{-LiBr-LiCl}$  Solid Solution. *Chem. Mater.* **2019**, *31*, 5133–5144. [[CrossRef](#)]
21. Kim, G.; Jhi, S.-H.; Park, N.; Louie, S.G.; Cohen, M.L. Optimization of Metal Dispersion in Doped Graphitic Materials for Hydrogen Storage. *Phys. Rev. B* **2008**, *78*, 085408. [[CrossRef](#)]
22. Kim, J.; Han, J.; Seo, M.; Kang, S.; Kim, D.; Ihm, J. High-Surface Area Ceramic-Derived Boron Nitride and Its Hydrogen Uptake Properties. *J. Mater. Chem. A* **2013**, *1*, 1014–1017. [[CrossRef](#)]
23. Bafekry, A.; Ghergherehchi, M.; Farjami Shayesteh, S.; Peeters, F.M. Adsorption of Molecules on  $\text{C}_3\text{N}$  Nanosheet: A First-Principles Calculations. *Chem. Phys.* **2019**, *526*, 110442. [[CrossRef](#)]
24. Duchêne, L.; Lunghammer, S.; Burankova, T.; Liao, W.-C.; Embs, J.P.; Coperet, C.; Wilkening, H.M.R.; Remhof, A.; Hagemann, H.; Battaglia, C. Ionic Conduction Mechanism in the  $\text{Na}_2(\text{B}_{12}\text{H}_{12})_{0.5}(\text{B}_{10}\text{H}_{10})_{0.5}$  Closo-Borate Solid-State Electrolyte: Interplay of Disorder and Ion–Ion Interactions. *Chem. Mater.* **2019**, *31*, 3449–3460. [[CrossRef](#)]
25. Ariharan, A.; Viswanathan, B.; Nandhakumar, V. Hydrogen Storage on Boron Substituted Carbon Materials. *Int. J. Hydrogen Energy* **2016**, *41*, 3527–3536. [[CrossRef](#)]
26. Murgia, F.; Brighi, M.; Cerny, R. Room-Temperature-Operating Na-Ion Solid-State Battery with Complex Hydride as Electrolyte. *Electrochem. Commun.* **2019**, *106*, 106534. [[CrossRef](#)]
27. Skripov, A.V.; Soloninin, A.V.; Babanova, O.A.; Skoryunov, R.V. Anion and Cation Dynamics in Polyhydroborate Salts: NMR Studies. *Molecules* **2020**, *25*, 2940. [[CrossRef](#)] [[PubMed](#)]
28. Wang, C.; Tang, C.; Fu, L. An Effective Method to Screen Carbon (Boron, Nitrogen) Based Two-Dimensional Hydrogen Storage Materials. *Int. J. Hydrogen Energy* **2020**, *45*, 25054–25064. [[CrossRef](#)]
29. Weng, Q. Porosity Engineering of Boron Nitride Materials for Hydrogen Storage. Ph.D. Dissertation, University of Tsukuba, Graduate School of Pure and Applied Sciences, Tsukuba, Japan, 2015. Available online: <http://hdl.handle.net/2241/00128908> (accessed on 10 April 2025).
30. Sakr, M.A.; Abdelsalam, H.; Teleb, N.H.; Abd-Elkader, O.H.; Zhang, Q. Exploring the Structural, Electronic, and Hydrogen Storage Properties of Hexagonal Boron Nitride and Carbon Nanotubes: Insights from Single-Walled to Doped Double-Walled Configurations. *Sci. Rep.* **2024**, *14*, 4970. [[CrossRef](#)]
31. Smidstrup, S.; Markussen, T.; Vanraeyveld, P.; Wellendorff, J.; Schneider, J.; Gunst, T.; Verstichel, B.; Stradi, D.; A Khomyakov, P.; Vej-Hansen, U.G.; et al. QuantumATK: An integrated platform of electronic and atomicscale modelling tools. *J. Phys. Condens. Matter* **2020**, *32*, 36. [[CrossRef](#)]
32. Segall, M.D.; Lindan, P.J.D.; Probert, M.J.; Pickard, C.J.; Hasnip, P.J.; Clark, S.J.; Payne, M.C. First-principles simulation: Ideas, illustrations and the CASTEP code. *J. Phys. Condens. Matter* **2002**, *14*, 2717–2744. [[CrossRef](#)]
33. Guest, M.F.; Bush, I.J.; Van Dam, H.J.J.; Sherwood, P.; Thomas, J.M.H.; Van Lenthe, J.H.; Havenith, R.W.A.; Kendrick, J. The GAMESS-UK electronic structure package: Algorithms, developments and applications. *Mol. Phys.* **2005**, *103*, 719–747. [[CrossRef](#)]
34. Ülgen, B.E.; Filiz, B.C.; Açıkalın, K.; Yörüklü, H.C.; Figen, A.K. Boron-Based Hydrogen Storage Materials for Highly Selective Hydrogenation to Liquid Organic Hydrogen Carriers Synthesis Focus on Formic Acid. *Int. J. Hydrogen Energy* **2024**, *in press*. [[CrossRef](#)]
35. Hafner, J. Materials simulations using VASP—a quantum perspective to materials science. *Comput. Phys. Commun.* **2007**, *177*, 6–13. [[CrossRef](#)]

36. Yoshida, K.; Sato, T.; Unemoto, A.; Matsuo, M.; Ikeshoji, T.; Udovic, T.J.; Orimo, S.I. Fast Sodium Ionic Conduction in Na<sub>2</sub>B<sub>10</sub>H<sub>10</sub>-Na<sub>2</sub>B<sub>12</sub>H<sub>12</sub> Pseudo-Binary Complex Hydride and Application to a Bulk-Type All-Solid-State Battery. *Appl. Phys. Lett.* **2017**, *110*, 103901. [[CrossRef](#)]
37. Hussain, T.; Islam, M.S.; Rao, G.S.; Panigrahi, P.; Gupta, D.; Ahuja, R. Hydrogen storage properties of light metal adatoms (Li, Na) decorated fluorographene monolayer. *Nanotechnology* **2015**, *26*, 275401. [[CrossRef](#)]
38. Weng, Q.; Zeng, L.; Chen, Z.; Han, Y.; Jiang, K.; Bando, Y.; Golberg, D. Hydrogen Storage in Carbon and Oxygen Co-Doped Porous Boron Nitrides. *Adv. Funct. Mater.* **2021**, *31*, 2007381. [[CrossRef](#)]
39. Panigrahi, P.; Naqvi, S.R.; Hankel, M.; Ahuja, R.; Hussain, T. Enriching the hydrogen storage capacity of carbon nanotube doped with polythiated molecules. *Appl. Surf. Sci.* **2018**, *444*, 467–473. [[CrossRef](#)]
40. Shao, H.; Felderhoff, M.; Schüth, F. Hydrogen storage properties of nanostructured MgH<sub>2</sub>/TiH<sub>2</sub> composite prepared by ball milling under high hydrogen pressure. *Int. J. Hydrogen Energy* **2011**, *36*, 10828–10833. [[CrossRef](#)]
41. Kozhakhmetov, Y.A.; Skakov, M.K.; Kurbanbekov, S.R.; Mukhamedov, N.M.; Mukhamedov, N.Y. Powder Composition Structurization of the Ti-25Al-25Nb (at.%) System upon Mechanical Activation and Subsequent Spark Plasma Sintering. *Eurasian Chem. Technol. J.* **2021**, *23*, 37–44. [[CrossRef](#)]
42. Zhanbolatova, G.K.; Baklanov, V.V.; Skakov, M.K.; Sokolov, I.A.; Bukina, O.S.; Kozhahmetov, Y.A.; Orazgaliev, N.A. Influence of Temperature on Tungsten Carbide Formation in a Beam Plasma Discharge. *J. Phys. Conf. Ser.* **2021**, *2064*, 012055. [[CrossRef](#)]
43. Skakov, M.; Miniyazov, A.; Batyrbekov, E.; Baklanov, V.; Koyanbayev, Y.; Gradoboev, A.; Kozhakhmetov, Y.; Sokolov, I.; Tulenbergenov, T.; Zhanbolatova, G. Influence of the Carbided Tungsten Surface on the Processes of Interaction with Helium Plasma. *Materials* **2022**, *15*, 7821. [[CrossRef](#)]
44. Salazar-Aparicio, R.V.; Vazquez-Nava, R.A.; Arzate, N.; Mendoza, B.S. Molecular hydrogen physisorption on boron-nitride nanotubes probed by second harmonic generation. *Phys. Rev. B* **2014**, *90*, 155403. [[CrossRef](#)]
45. Lim, S.H.; Luo, J.; Ji, W.; Lin, J. Synthesis of boron nitride nanotubes and its hydrogen uptake. *Catal. Today* **2007**, *120*, 346–350. [[CrossRef](#)]
46. Wang, Y.; Wang, F.; Xu, B.; Zhang, J.; Sun, Q.; Jia, Y. Theoretical prediction of hydrogen storage on Li-decorated boron nitride atomic chains. *J. Appl. Phys.* **2013**, *113*, 064309. [[CrossRef](#)]
47. Moussa, G.; Demirci, U.B.; Malo, S.; Bernard, S.; Miele, P. Hollow core mesoporous shell boron nitride nanopolyhedron-confined ammonia borane: A pure B–N–H composite for chemical hydrogen storage. *J. Mater. Chem. A* **2014**, *2*, 7717–7722. [[CrossRef](#)]
48. Moussa, G.; Salameh, C.; Bruma, A.; Malo, S.; Demirci, U.B.; Bernard, S.; Miele, P. Nanostructured boron nitride: From molecular design to hydrogen storage application. *Inorganics* **2014**, *2*, 396–409. [[CrossRef](#)]
49. Hamilton, C.W.; Baker, R.T.; Staubitz, A.; Manners, I. B–N compounds for chemical hydrogen storage. *Chem. Soc. Rev.* **2009**, *38*, 279–293. [[CrossRef](#)]
50. Revabhai, P.M.; Singhal, R.K.; Basu, H.; Kailasa, S.K. Progress on boron nitride nanostructure materials: Properties, synthesis and applications in hydrogen storage and analytical chemistry. *J. Nanostruct. Chem.* **2023**, *13*, 1–41. [[CrossRef](#)]
51. Brighi, M.; Murgia, F.; Cerny, R. Closo-Hydroborate Sodium Salts as an Emerging Class of Room-Temperature Solid Electrolytes. *Cell Rep. Phys. Sci.* **2020**, *1*, 100217. [[CrossRef](#)]
52. Wang, J.; Ma, F.; Sun, M. Graphene, hexagonal boron nitride, and their heterostructures: Properties and applications. *RSC Adv.* **2017**, *7*, 16801–16822. [[CrossRef](#)]
53. Jepsen, L.H.; Ley, M.B.; Lee, Y.S.; Cho, Y.W.; Dornheim, M.; Jensen, J.O.; Jensen, T.R. Boron–nitrogen based hydrides and reactive composites for hydrogen storage. *Mater. Today* **2014**, *17*, 129–135. [[CrossRef](#)]
54. Chopra, N.G.; Luyken, R.J.; Cherrey, K.; Crespi, V.H.; Cohen, M.L.; Louie, S.G.; Zettl, A. Boron Nitride Nanotubes. *Science* **1995**, *269*, 966–967. [[CrossRef](#)]
55. Rubio, A.; Corkill, J.L.; Cohen, M.L. Theory of graphitic boron nitride nanotubes. *Phys. Rev. B* **1994**, *49*, 5081–5084. [[CrossRef](#)] [[PubMed](#)]
56. Blase, X.; Rubio, A.; Louie, S.G.; Cohen, M.L. Stability and Band Gap Constancy of Boron Nitride Nanotubes. *Europhys. Lett.* **1994**, *28*, 335–340. [[CrossRef](#)]
57. Li, Y.; Zhou, Z.; Golberg, D.; Bando, Y.; von Ragué Schleyer, P.; Chen, Z. Stone–Wales defects in single-walled boron nitride nanotubes: Formation energies, electronic structures, and reactivity. *J. Phys. Chem. C* **2008**, *112*, 1365–1370. [[CrossRef](#)]
58. Choyal, V.; Kundalwal, S.I. Effect of Stone–Wales defects on the mechanical behavior of boron nitride nanotubes. *Acta Mech.* **2020**, *231*, 4003–4018. [[CrossRef](#)]
59. Kalay, S.; Yilmaz, Z.; Sen, O.; Emanet, M.; Kazanc, E.; Çulha, M. Synthesis of boron nitride nanotubes and their applications. *Beilstein J. Nanotechnol.* **2015**, *6*, 84–102. [[CrossRef](#)]
60. Pakdel, A.; Zhi, C.; Bando, Y.; Nakayama, N.; Golberg, D. A comprehensive analysis of the CVD growth of boron nitride nanotubes. *Nanotechnology* **2012**, *23*, 215601. [[CrossRef](#)]
61. Guo, C.; Wang, C. Strategies for Enhancing Hydrogen Storage Capacity of Carbon-Based Sandwich Material by Boron Doping: Exploring the Optimal Doping Ratio. *J. Energy Storage* **2024**, *97*, 112915. [[CrossRef](#)]

62. Singhal, S.K.; Srivastava, A.K.; Pasricha, R.; Mathur, R.B. Fabrication of Al-Matrix Composites Reinforced with Amino Functionalized Boron Nitride Nanotubes. *J. Nanosci. Nanotechnol.* **2011**, *11*, 5179–5186. [[CrossRef](#)]
63. Wu, J.; Yin, L. Platinum Nanoparticle Modified Polyaniline-Functionalized Boron Nitride Nanotubes for Amperometric Glucose Enzyme Biosensor. *ACS Appl. Mater. Interfaces* **2011**, *3*, 4354–4362. [[CrossRef](#)]
64. Chen, H.; Chen, Y.; Liu, Y.; Fu, L.; Huang, C.; Llewellyn, D. Over 1.0 mm-Long Boron Nitride Nanotubes. *Chem. Phys. Lett.* **2008**, *463*, 130–133. [[CrossRef](#)]
65. Samanta, S.K.; Gomathi, A.; Bhattacharya, S.; Rao, C.N.R. Novel Nanocomposites Made of Boron Nitride Nanotubes and a Physical Gel. *Langmuir* **2010**, *26*, 12230–12236. [[CrossRef](#)] [[PubMed](#)]
66. Li, L.H.; Chen, Y. Superhydrophobic Properties of Nonaligned Boron Nitride Nanotube Films. *Langmuir* **2010**, *26*, 5135–5140. [[CrossRef](#)]
67. Chen, Y.; Conway, M.; Williams, J.S.; Lefler, M.; Zhi, C.; Han, W.; Chai, G. Large-Quantity Production of High-Yield Boron Nitride Nanotubes. *J. Mater. Res.* **2002**, *17*, 1896–1899. [[CrossRef](#)]
68. Yamaguchi, M.; Pakdel, A.; Zhi, C.; Bando, Y.; Golberg, D. Utilization of Multiwalled Boron Nitride Nanotubes for the Reinforcement of Lightweight Aluminum Ribbons. *Nanoscale Res. Lett.* **2013**, *8*, 3. [[CrossRef](#)]
69. Özmen, D.; Sezgi, N.A.; Balci, S. Synthesis of Boron Nitride Nanotubes from Ammonia and a Powder Mixture of Boron and Iron Oxide. *Chem. Eng. J.* **2013**, *219*, 28–36. [[CrossRef](#)]
70. Zhou, S.-J.; Ma, C.-Y.; Meng, Y.-Y.; Su, H.-F.; Zhu, Z.; Deng, S.-L.; Xie, S.-Y. Activation of Boron Nitride Nanotubes and Their Polymer Composites for Improving Mechanical Performance. *Nanotechnology* **2012**, *23*, 055708. [[CrossRef](#)] [[PubMed](#)]
71. Zhong, B.; Huang, X.; Wen, G.; Li, M.; Liu, D.; Xu, S.; Wang, C.; Zhi, C.; Tang, D. Large-Scale Fabrication of Boron Nitride Nanotubes via a Facile Chemical Vapor Reaction Route and Their Cathodoluminescence Properties. *Nanoscale Res. Lett.* **2011**, *6*, 36. [[CrossRef](#)]
72. Saner Okan, B.; Kocabaş, Z.Ö.; Nalbant Ergün, A.; Baysal, M.; Letofsky-Papst, I.; Yürüm, Y. Effect of Reaction Temperature and Catalyst Type on the Formation of Boron Nitride Nanotubes by Chemical Vapor Deposition and Measurement of Their Hydrogen Storage Capacity. *Ind. Eng. Chem. Res.* **2012**, *51*, 11341–11347. [[CrossRef](#)]
73. Narita, I.; Oku, T. Synthesis of Boron Nitride Nanotubes by Using YB<sub>6</sub> Powder. *Solid. State Commun.* **2002**, *123*, 395–398. [[CrossRef](#)]
74. Chai, L.; Chen, K.; Zhi, Y.; Murty, K.L.; Chen, L.-Y.; Yang, Z. Nanotwins Induced by Pulsed Laser and Their Hardening Effect in a Zr Alloy. *J. Alloys Compd.* **2018**, *750*, 443–450. [[CrossRef](#)]
75. Abbasov, G.D.; Tahirli, H.M.; Verdiev, S.C.; Mammadova, S.A.; Shirinov, T.I.; Guliyeva, L.; Museyibli, K.; Adigozalova, M.N.; Rustamova, S.M.; Huseynova, A.S. Corrosion of Carbon Steel and Some Other Metals in Fresh Water of Hydraulic Structures. *Chem. Probl.* **2024**, *22*, 516–524. [[CrossRef](#)]
76. Rakhadilov, B.K.; Kurbanbekov, S.R.; Kilishkhanov, M.K.; Kenesbekov, A.B.; Amanzholov, S. Changing the Structure and Phase States and the Microhardness of the R<sub>6</sub>M<sub>5</sub> Steel Surface Layer after Electrolytic-Plasma Nitriding. *Eurasian J. Phys. Funct. Mater.* **2018**, *2*, 259–266. [[CrossRef](#)]
77. Kengesbekov, A. Influence of Plasma Arc Current and Gas Flow on the Structural and Tribological Properties of TiN Coatings Obtained by Plasma Spraying. *Coatings* **2024**, *14*, 1404. [[CrossRef](#)]
78. Rakhadilov, B.; Kenesbekov, A.; Skakov, M.; Miniyzov, A. Hydrogen and Deuterium Storage in Tungsten When Irradiation with Plasma Beam. In Proceedings of the METAL 2018–27th International Conference on Metallurgy and Materials, Conference Proceedings, Ostrva, Czech Republic, 23–25 May 2018; pp. 1216–1221.
79. Zhu, J.; Wang, H.; Cai, W.; Liu, J.; Ouyang, L.; Zhu, M. The Milled LiBH<sub>4</sub>/h-BN Composites Exhibiting Unexpected Hydrogen Storage Kinetics and Reversibility. *Int. J. Hydrogen Energy* **2017**, *42*, 15790–15798. [[CrossRef](#)]
80. Muthu, R.N.; Rajashabala, S.; Kannan, R. Hydrogen Storage Performance of Lithium Borohydride Decorated Activated Hexagonal Boron Nitride Nanocomposite for Fuel Cell Applications. *Int. J. Hydrogen Energy* **2017**, *42*, 15586–15596. [[CrossRef](#)]
81. Tu, G.; Xiao, X.; Jiang, Y.; Qin, T.; Li, S.; Ge, H.; Wang, Q.; Chen, L. Composite cooperative enhancement on the hydrogen desorption kinetics of LiBH<sub>4</sub> by co-doping with NbCl<sub>5</sub> and hexagonal BN. *Int. J. Hydrogen Energy* **2015**, *40*, 10527–10535. [[CrossRef](#)]
82. Ma, Y.; Li, Y.; Liu, T.; Zhao, X.; Zhang, L.; Han, S.; Wang, Y. Enhanced hydrogen storage properties of LiBH<sub>4</sub> generated using a porous Li<sub>3</sub>BO<sub>3</sub> catalyst. *J. Alloys Compd.* **2016**, *689*, 187–191. [[CrossRef](#)]
83. Li, Z.; Gao, M.; Gu, J.; Xian, K.; Yao, Z.; Shang, C.; Liu, Y.; Guo, Z.; Pan, H. In situ introduction of Li<sub>3</sub>BO<sub>3</sub> and NbH leads to superior cyclic stability and kinetics of a LiBH<sub>4</sub>-based hydrogen storage system. *ACS Appl. Mater. Interfaces* **2020**, *12*, 893–903. [[CrossRef](#)]
84. Wu, Y.; Jiang, X.; Chen, J.; Qi, Y.; Zhang, Y.; Fu, H.; Zheng, J.; Li, X. Boric acid destabilized lithium borohydride with a 5.6 wt% dehydrogenation capacity at moderate temperatures. *Dalton Trans.* **2017**, *46*, 4499–4503. [[CrossRef](#)]
85. Roedern, E.; Hansen, B.R.S.; Ley, M.B.; Jensen, T.R. Effect of eutectic melting, reactive hydride composites, and nanoconfinement on decomposition and reversibility of LiBH<sub>4</sub>-KBH<sub>4</sub>. *J. Phys. Chem. C* **2015**, *119*, 25818–25825. [[CrossRef](#)]

86. Matus, M.H.; Anderson, K.D.; Camaioni, D.M.; Autrey, S.T.; Dixon, D.A. Reliable Predictions of the Thermochemistry of Boron–Nitrogen Hydrogen Storage Compounds:  $B_xN_xH_y$ ,  $x = 2, 3$ . *J. Phys. Chem. A* **2007**, *111*, 4411–4421. [[CrossRef](#)]
87. Frommen, C.; Heere, M.; Riktor, M.D.; Sørby, M.H.; Hauback, B.C. Hydrogen storage properties of rare earth (RE) borohydrides (RE = La, Er) in composite mixtures with  $LiBH_4$  and  $LiH$ . *J. Alloys Compd.* **2015**, *645*, S155–S159. [[CrossRef](#)]
88. Liu, Y.; Reed, D.; Paterakis, C.; Contreras Vasquez, L.; Baricco, M.; Book, D. Study of the decomposition of a  $0.62LiBH_4$ – $0.38NaBH_4$  mixture. *Int. J. Hydrogen Energy* **2017**, *42*, 22480–22488. [[CrossRef](#)]
89. Lohstroh, W.; Heere, M. Structure and Dynamics of Borohydrides Studied by Neutron Scattering Techniques: A Review. *J. Phys. Soc. Jpn.* **2020**, *89*, 1–12. [[CrossRef](#)]
90. Liu, Y.; Liu, W.; Wang, R.; Hao, L.; Jiao, W. Hydrogen storage using Na-decorated graphyne and its boron nitride analog. *Int. J. Hydrogen Energy* **2014**, *39*, 12757–12764. [[CrossRef](#)]
91. Weidenthaler, C.; Pommerin, A.; Felderhoff, M.; Sun, W.; Wolverson, C.; Bogdanovic, B.; Schuth, F. Complex rare-earth aluminum hydrides: Mechanochemical preparation, crystal structure and potential for hydrogen storage. *J. Am. Chem. Soc.* **2009**, *131*, 16735–16743. [[CrossRef](#)]
92. Hagemann, H. Boron Hydrogen Compounds for Hydrogen Storage and As Solid Ionic Conductors. *Chimia* **2019**, *73*, 868. [[CrossRef](#)]
93. Chen, X.; Liu, X.-R.; Wang, X.; Chen, X.-M.; Jing, Y.; Wie, D. A Safe and Efficient Synthetic Method of the Alkali Metal Octahydrotriborate, Unravelling a General Mechanism of Constructing the Delta B3 Unit of Polyhedral Boranes. *Dalton Trans.* **2021**, *50*, 13676–13679. [[CrossRef](#)]
94. Chen, X.-M.; Ma, N.; Zhang, Q.-F.; Wang, J.; Feng, X.; Wei, C.; Wang, L.-S.; Zhang, J.; Chen, X. Elucidation of the Formation Mechanisms of the Octahydrotriborate Anion ( $B_3H_8^-$ ) through the Nucleophilicity of the B–H Bond. *J. Am. Chem. Soc.* **2018**, *140*, 6718–6726. [[CrossRef](#)]
95. Moury, R.; Gigante, A.; Hagemann, H. An alternative approach to the synthesis of  $NaB_3H_8$  and  $Na_2B_{12}H_{12}$  for solid electrolyte applications. *Int. J. Hydrogen Energy* **2017**, *42*, 22417–22421. [[CrossRef](#)]
96. Hagemann, H. Boron Hydrogen Compounds: Hydrogen Storage and Battery Applications. *Molecules* **2021**, *26*, 7425. [[CrossRef](#)] [[PubMed](#)]
97. Yan, Y.; Remhof, A.; Rentsch, D.; Züttel, A. The role of  $MgB_{12}H_{12}$  in the hydrogen desorption process of  $Mg(BH_4)_2$ . *Chem. Commun.* **2015**, *51*, 700–702. [[CrossRef](#)] [[PubMed](#)]
98. Paskevicius, M.; Pitt, M.P.; Brown, D.H.; Sheppard, D.A.; Chumphongphan, S.; Buckley, C.E. First-order phase transition in the  $Li_2B_{12}H_{12}$  system. *Phys. Chem. Chem. Phys.* **2013**, *15*, 15825–15828. [[CrossRef](#)] [[PubMed](#)]
99. Nguyen, M.T.; Matus, M.H.; Dixon, D.A. Heats of Formation of Boron Hydride Anions and Dianions and Their Ammonium Salts  $[B_nH_m^{y-}][NH_4^+]_y$  with  $y = 1–2$ . *Inorg. Chem.* **2007**, *46*, 7561–7570. [[CrossRef](#)]
100. Kelley, S.P.; McCrary, P.D.; Flores, L.; Garner, E.B.; Dixon, D.A.; Rogers, R.D. Structural and Theoretical Study of Salts of the  $[B_9H_{14}]^-$  Ion: Isolation of Multiple Isomers and Implications for Energy Storage. *ChemPlusChem* **2016**, *81*, 922–925. [[CrossRef](#)]
101. Sethio, D.; Lawson Daku, L.M.; Hagemann, H.; Kraka, E. Quantitative Assessment of B–B–B, B–Hb–B, and B–Ht Bonds: From  $BH_3$  to  $B_{12}H_{12}^{2-}$ . *ChemPhysChem* **2019**, *20*, 1967–1977. [[CrossRef](#)]
102. Maillard, R.; Sethio, D.; Hagemann, H.; Lawson Daku, L.M. Accurate Computational Thermodynamics Using Anharmonic Density Functional Theory Calculations: The Case Study of B–H Species. *ACS Omega* **2019**, *4*, 8786–8794. [[CrossRef](#)]
103. Lee, T.B.; Mc Kee, M.L. Redox Energetics of Hypercloso Boron Hydrides  $B_nH_n$  ( $n = 6–13$ ) and  $B_{12}X_{12}$  ( $X = F, Cl, OH, \text{ and } CH_3$ ). *Inorg. Chem.* **2012**, *51*, 4205–4214. [[CrossRef](#)]
104. Lee, T.B.; Mc Kee, M.L. Dissolution Thermochemistry of Alkali Metal Dianion Salts ( $M_2X_1$ ,  $M = Li^+, Na^+, \text{ and } K^+$  with  $X = CO_3^{2-}, SO_4^{2-}, C_8H_8^{2-}, \text{ and } B_{12}H_{12}^{2-}$ ). *Inorg. Chem.* **2011**, *50*, 11412–11422. [[CrossRef](#)]
105. Cheng, J.; Zhang, L.; Ding, R.; Ding, Z.; Wang, X.; Wang, Z. Grand canonical Monte Carlo simulation of hydrogen physisorption in single-walled boron nitride nanotubes. *Int. J. Hydrogen Energy* **2007**, *32*, 3402–3405. [[CrossRef](#)]
106. Liu, C.; Chen, Y.; Wu, C.Z.; Xu, S.T.; Cheng, H.M. Hydrogen Storage in Carbon Nanotubes Revisited. *Carbon* **2010**, *48*, 452–455. [[CrossRef](#)]
107. Aliyeva, N.A.; Sardarly, R.M.; Gadzhieva, N.N.; Gakhramanova, S.M.; Mammadov, R.A. Radiation-Stimulated Conversion to Superionic State of TlSe and TlS Crystals. *Probl. At. Sci. Technol.* **2024**, *2024*, 23–28. [[CrossRef](#)]
108. Grochala, W.; Edwards, P.P. Thermal Decomposition of the Non-Interstitial Hydrides for the Storage and Production of Hydrogen. *Chem. Rev.* **2004**, *104*, 1283–1315. [[CrossRef](#)]
109. Reiser, A.; Bogdanović, B.; Schlichte, K. The Application of Mg-Based Metal-Hydrides as Heat Energy Storage Systems. *Int. J. Hydrogen Energy* **2000**, *25*, 425–430. [[CrossRef](#)]
110. Dehouche, Z.; Klassen, T.; Oelerich, W.; Goyette, J.; Bose, T.K.; Schulz, R. Cycling and Thermal Stability of Nanostructured  $MgH_2$ – $Cr_2O_3$  Composite for Hydrogen Storage. *J. Alloys Compd.* **2002**, *347*, 319–323. [[CrossRef](#)]
111. Huot, J.; Liang, G.; Boily, S.; Van Neste, A.; Schulz, R. Structural Study and Hydrogen Sorption Kinetics of Ball-Milled Magnesium Hydride. *J. Alloys Compd.* **1999**, *293–295*, 495–500. [[CrossRef](#)]

112. Imamura, H.; Masanari, K.; Kusuvara, M.; Katsumoto, H.; Sumi, T.; Sakata, Y. High hydrogen storage capacity of nanosized magnesium synthesized by high energy ball-milling. *J. Alloys Compd.* **2005**, *386*, 211–216. [[CrossRef](#)]
113. Zhou, W.; Yang, P.; Tian, Y.; Li, Y.; Wang, C. Hydrogen Storage on Transition-Metal-Decorated Boron Nitride Nanotubes: A First-Principles Study. *J. Phys. Chem. C* **2011**, *115*, 553–560. [[CrossRef](#)]
114. Jhi, S.H.; Kwon, Y.K. Hydrogen adsorption on boron nitride nanotubes: A path to room-temperature hydrogen storage. *Phys. Rev. B Condens. Matter Mater. Phys.* **2004**, *69*, 245407–245414. [[CrossRef](#)]
115. Bae, S.Y.; Seo, H.W.; Park, J.; Choi, Y.S.; Park, J.C.; Lee, S.Y. Boron nitride nanotubes synthesized in the temperature range 1000–1200 °C. *Chem. Phys. Lett.* **2003**, *374*, 534–541. [[CrossRef](#)]
116. Wu, X.; Yang, J.L.; Zeng, X.C. Adsorption of hydrogen molecules on the platinum-doped boron nitride nanotubes. *J. Chem. Phys.* **2006**, *125*, 44704. [[CrossRef](#)]
117. Banerjee, P.; Pathak, B.; Ahuja, R.; Das, G.P. First Principles Design of Li Functionalized Hydrogenated h-BN Nanosheet for Hydrogen Storage. *Int. J. Hydrogen Energy* **2016**, *41*, 14437–14446. [[CrossRef](#)]
118. Gigante, A.; Leick, N.; Lipton, A.S.; Tran, B.; Strange, N.A.; Bowden, M.; Martinez, M.B.; Moury, R.; Gennett, T.; Hagemann, H.; et al. Thermal Conversion of Unsolvated  $Mg(B_3H_8)_2$  to  $BH_4^-$  in the Presence of  $MgH_2$ . *ACS Appl. Energy Mater.* **2021**, *4*, 3737–3747. [[CrossRef](#)] [[PubMed](#)]
119. Kondo, T.; Shindo, K.; Sakurai, Y. Comparison of hydrogen absorption properties of Ti mechanically milled with hexagonal boron nitride (h-BN) and with graphite. *J. Alloys Compd.* **2005**, *386*, 202–206. [[CrossRef](#)]
120. Chen, M.; Zhao, Y.J.; Liao, J.H.; Bao, Y.X. Transition-Metal Dispersion on Carbon-Doped Boron Nitride Nanostructures: Applications for High-Capacity Hydrogen Storage. *Phys. Rev. B* **2012**, *86*, 045459–45467. [[CrossRef](#)]
121. He, L.; Wang, H.; Chen, L.; Wang, X.; Xie, H.; Jiang, C.; Li, C.; Elibol, K.; Meyer, J.; Watanabe, K.; et al. Isolating Hydrogen in Hexagonal Boron Nitride Bubbles by a Plasma Treatment. *Nat. Commun.* **2019**, *10*, 2815–2819. [[CrossRef](#)] [[PubMed](#)]
122. Kovalskii, A.M.; Manakhov, A.M.; Afanasev, P.A.; Popov, Z.I.; Matveev, A.T.; Al-Qasim, A.S. Hydrogen Storage Ability of Hexagonal Boron Nitride. *Front. Mater.* **2024**, *11*, 1375977. [[CrossRef](#)]
123. Ma, R.; Bando, Y.; Sato, T.; Golberg, D.; Zhu, H.; Xu, C.; Wu, D. Synthesis of Boron Nitride Nanofibers and Measurement of Their Hydrogen Uptake Capacity. *Appl. Phys. Lett.* **2002**, *81*, 5225–5227. [[CrossRef](#)]
124. Ma, R.; Bando, Y.; Zhu, H.; Sato, T.; Xu, C.; Wu, D. Hydrogen Uptake in Boron Nitride Nanotubes at Room Temperature. *J. Am. Chem. Soc.* **2002**, *124*, 7672–7673. [[CrossRef](#)]
125. Leela, A.; Reddy, M.; Tanur, A.E.; Walker, G.C. Synthesis and Hydrogen Storage Properties of Different Types of Boron Nitride Nanostructures. *Int. J. Hydrogen Energy* **2010**, *35*, 4138–4143. [[CrossRef](#)]
126. Wang, P.; Orimo, S.; Matsushima, T.; Fujii, H.; Majer, G. Hydrogen in Mechanically Prepared Nanostructured h-BN: A Critical Comparison with That in Nanostructured Graphite. *Appl. Phys. Lett.* **2002**, *80*, 318–320. [[CrossRef](#)]
127. Tang, C.; Bando, Y.; Ding, X.; Qi, S.; Golberg, D. Catalyzed Collapse and Enhanced Hydrogen Storage of BN Nanotubes. *J. Am. Chem. Soc.* **2002**, *124*, 14550–14551. [[CrossRef](#)] [[PubMed](#)]
128. Lei, W.; Zhang, H.; Wu, Y.; Zhang, B.; Liu, D.; Qin, S.; Liu, Z.; Liu, L.; Ma, Y.; Chen, Y. Oxygen-Doped Boron Nitride Nanosheets with Excellent Performance in Hydrogen Storage. *Nano Energy* **2014**, *6*, 219–224. [[CrossRef](#)]
129. Weng, Q.; Wang, X.; Bando, Y.; Golberg, D. One-Step Template-Free Synthesis of Highly Porous Boron Nitride Microsponges for Hydrogen Storage. *Adv. Energy Mater.* **2014**, *4*, 1301525. [[CrossRef](#)]
130. Li, J.; Lin, J.; Xu, X.; Zhang, X.; Xue, Y.; Mi, J.; Mo, Z.; Fan, Y.; Hu, L.; Yang, X.; et al. Porous Boron Nitride with a High Surface Area: Hydrogen Storage and Water Treatment. *Nanotechnology* **2013**, *24*, 155603. [[CrossRef](#)]
131. Weng, Q.; Wang, X.; Zhi, C.; Bando, Y.; Golberg, D. Boron Nitride Porous Microbelts for Hydrogen Storage. *ACS Nano* **2013**, *7*, 1558–1565. [[CrossRef](#)]
132. Tokarev, A.; Kjeang, E.; Cannon, M.; Bessarabov, D. Theoretical Limit of Reversible Hydrogen Storage Capacity for Pristine and Oxygen-Doped Boron Nitride. *Int. J. Hydrogen Energy* **2016**, *41*, 16984–16991. [[CrossRef](#)]
133. Ren, J.; Zhang, N.; Zhang, H.; Peng, X. First-Principles Study of Hydrogen Storage on Pt (Pd)-Doped Boron Nitride Sheet. *Struct. Chem.* **2015**, *26*, 731–738. [[CrossRef](#)]
134. Zhang, H.; Tong, C.J.; Zhang, Y.; Zhang, Y.N.; Liu, L.M. Porous BN for Hydrogen Generation and Storage. *J. Mater. Chem. A* **2015**, *3*, 9632–9637. [[CrossRef](#)]
135. Shahsavari, R.; Zhao, S. Merger of Energetic Affinity and Optimal Geometry Provides New Class of Boron Nitride Based Sorbents with Unprecedented Hydrogen Storage Capacity. *Small* **2018**, *14*, 1702863. [[CrossRef](#)]
136. Zhang, N.; Shi, Y.; Li, J.; Zhang, Y.; Guo, J.; Fu, Z.; Zhang, P. Potential Applications of  $OLi_3$ -Decorated h-BN Monosheet for High Hydrogen Storage. *Appl. Phys. Lett.* **2023**, *123*, 83902. [[CrossRef](#)]
137. Rai, D.P.; Chettri, B.; Patra, P.K.; Sattar, S. Hydrogen Storage in Bilayer Hexagonal Boron Nitride: A First-Principles Study. *ACS Omega* **2021**, *6*, 30362–30370. [[CrossRef](#)] [[PubMed](#)]

138. Chettri, B.; Patra, P.K.; Srivastava, S.; Laref, A.; Rai, D.P. Enhanced H<sub>2</sub> Storage Capacity of Bilayer Hexagonal Boron Nitride (h-BN) Incorporating Van Der Waals Interaction under an Applied External Electric Field. *ACS Omega* **2021**, *6*, 22374–22382. [[CrossRef](#)]
139. Fu, P.; Wang, J.; Jia, R.; Bibi, S.; Eglitis, R.I.; Zhang, H.X. Theoretical Study on Hydrogen Storage Capacity of Expanded h-BN Systems. *Comput. Mater. Sci.* **2017**, *139*, 335–340. [[CrossRef](#)]
140. Chodvadiya, D.; Kanabar, S.; Chakraborty, B.; Jha, P.K. Exploring the Hydrogen Storage Possibility of the Pristine, Defected, and Metals Decorated o-B<sub>2</sub>N<sub>2</sub> Monolayers: Insights from DFT Simulations. *Int. J. Hydrogen Energy* **2024**, *53*, 958–968. [[CrossRef](#)]
141. Zhao-Karger, Z.; Silvi, L.; Petry, W.; Lohstroh, W. A Quasielastic and Inelastic Neutron Scattering Study of the Alkaline and Alkaline-Earth Borohydrides LiBH<sub>4</sub> and Mg(BH<sub>4</sub>)<sub>2</sub> and the Mixture LiBH<sub>4</sub> + Mg(BH<sub>4</sub>)<sub>2</sub>. *Phys. Chem. Chem. Phys.* **2019**, *21*, 718–728. [[CrossRef](#)]
142. Roy, L.; Bhunya, S.; Paul, A. A Metal-Free Strategy to Release Chemisorbed H<sub>2</sub> from Hydrogenated Boron Nitride Nanotubes. *Angew. Chem. Int. Ed.* **2014**, *53*, 12430–12435. [[CrossRef](#)] [[PubMed](#)]
143. Qiu, N.X.; Zhang, C.H.; Xue, Y. Tuning Hydrogen Storage in Lithium Functionalized BC<sub>2</sub>N Sheets by Doping with Boron and Carbon. *ChemPhysChem* **2014**, *15*, 3015–3025. [[CrossRef](#)]
144. Kinal, A.; Sayhan, S. Accurate Prediction of Hydrogen Storage Capacity of Small Boron Nitride Nanocages by Dispersion Corrected Semi-Empirical PM6-DH2 Method. *Int. J. Hydrogen Energy* **2016**, *41*, 392–400. [[CrossRef](#)]
145. Zhao, J.; Huo, Z.; Xu, S.; Xiong, M.; Liu, D.; Wang, Y.; Jia, X. Novel Functional Materials of Hydrogen Storage B<sub>20</sub>N<sub>24</sub>: A First-Principles Calculation. *Crystals* **2023**, *13*, 1029. [[CrossRef](#)]
146. Grinderslev, J.B.; Møller, K.T.; Yan, Y.; Chen, X.-M.; Li, Y.; Li, H.-W.; Zhou, W.; Skibsted, J.; Chen, X.; Jensen, T.R. Potassium Octahydridotriborate: Diverse Polymorphism in a Potential Hydrogen Storage Material and Potassium Ion Conductor. *Dalton Trans.* **2019**, *48*, 8872–8881. [[CrossRef](#)]
147. Cao, D.; Lan, J.; Wang, W.; Smit, B. Lithium-Doped 3D Covalent Organic Frameworks: High-Capacity Hydrogen Storage Materials. *Angew. Chem. Int. Ed.* **2009**, *48*, 4730–4733. [[CrossRef](#)] [[PubMed](#)]

**Disclaimer/Publisher's Note:** The statements, opinions and data contained in all publications are solely those of the individual author(s) and contributor(s) and not of MDPI and/or the editor(s). MDPI and/or the editor(s) disclaim responsibility for any injury to people or property resulting from any ideas, methods, instructions or products referred to in the content.